DOI: 10.1002/cmdc.201500428

Identification of Aminoimidazole and Aminothiazole Derivatives as Src Family Kinase Inhibitors

Cinzia Maria Francini,[a] Anna Lucia Fallacara,[b] Roberto Artusi,*[a] Laura Mennuni,[c] Alessia Calgani,[d] Adriano Angelucci,[d] Silvia Schenone,*[e] and Maurizio Botta[b, f]

Src family kinases (SFKs) are a family of non-receptor tyrosine kinases (TKs) implicated in the regulation of many cellular processes. The aberrant activity of these TKs has been associated with the growth and progression of cancer. In particular, c-Src is overexpressed or hyperactivated in a variety of solid tumors and is most likely a strong promoting factor for the development of metastasis. Herein, the synthesis of new 4-aminoimidazole and 2-aminothiazole derivatives and their in vitro biological evaluation are described for their potential use as SFK inhibitors. Initially, 2-aminothiazole analogues of dasatinib and 4-aminoimidazole derivatives were synthesized and tested against the SFKs Src, Fyn, Lyn, and Yes. Five hits were identified as the most promising compounds, with K_i values in the range of 90–480 nM. A combination of molecular docking, homology modeling, and molecular dynamics were then used to investigate the possible binding mode of such compounds within the ATP binding site of the SFKs. Finally, the antiproliferative activities of the best candidates were evaluated against SH-SY5Y and K562 cell lines. Compound **3b** [2-(4-{2-methyl-6-[(5-phenylthiazol-2-yl)amino]pyrimidin-4-yl}piperazin-1-yl)ethanol] was found to be the most active inhibitor.

Introduction

Tyrosine kinases (TKs) are key enzymes in cell signaling pathways that are responsible for cell growth, proliferation, adhesion, differentiation, and apoptosis.[1] It has been conclusively demonstrated that TK alterations (especially hyperactivation, hyperproduction, or mutations) that lead to disruption of cell signaling cascades play important roles in several diseases including cancer, inflammation, neurological disorders, and diabetes.[2] For this reason, TKs have become one of the major drug targets of the 21st Century. So far, more than 20 small-molecule TK inhibitors have been approved for the treatment of various diseases.[3]

[a] *Dr. C. M. Francini, Dr. R. Artusi*
Medicinal Chemistry Division, Rottapharm Biotech S.r.l.
Valosa di Sopra N 9 Street, 20900 Monza (Italy)
E-mail: roberto.artusi@rottapharmbiotech.com

[b] *Dr. A. L. Fallacara, Prof. M. Botta*
Dipartimento di Biotecnologie, Chimica e Farmacia
Università degli Studi di Siena, Via Aldo Moro 2, 53100 Siena (Italy)

[c] *Dr. L. Mennuni*
Pharmacology and Toxicology Division, Rottapharm Biotech S.r.l.
Valosa di Sopra N 9 Street, 20900 Monza (Italy)

[d] *Dr. A. Calgani, Dr. A. Angelucci*
Dipartimento di Scienze Cliniche Applicate e Biotecnologie
Università dell'Aquila, Via Vetoio Coppito, 67100 L'Aquila (Italy)

[e] *Prof. S. Schenone*
Dipartimento di Farmacia, Università degli Studi di Genova
Viale Benedetto XV, 3, 16132 Genova (Italy)
E-mail: schensil@unige.it

[f] *Prof. M. Botta*
Sbarro Institute for Cancer Research and Molecular Medicine
Center for Biotechnology, College of Science and Technology
Temple University, BioLife Science Building, Suite 333
1900 North 12th Street, Philadelphia, PA 19122 (USA)

c-Src is a cytoplasmic TK belonging to the Src family kinases (SFKs), which include nine members (c-Src, Fyn, Yes, Fgr, Lck, Hck, Blk, Lyn, and Frk). Their distribution is not the same in all tissues and cell types. In fact, Src, Fyn, and Yes are ubiquitously expressed, whereas the other members are generally localized in hematopoietic cells. However, SFKs present a conserved domain organization that includes an N-terminal Src homology domain (SH4), followed by a "unique region", two Src homology domains (SH2 and SH3), a polyproline type II (PPII) domain, a catalytic domain (SH1), and a short C-terminal tail. SH2 and SH3 domains both play a part in protein–protein interactions. The catalytic domain, responsible for TK activity, is formed by a bi-lobed structure, like all canonical kinases, with a small N-terminal lobe and a large C-terminal lobe, which form the ATP- and substrate-binding site at the inter-lobe cleft. The flexible chain that connects the N and C lobes is called the hinge region.[4]

These enzymes can be switched from inactive to active by control of their phosphorylation state and through protein interactions.[5] c-Src is overexpressed or hyperactivated in many solid tumors,[6] including colon, breast, liver, and pancreatic cancer, where its expression correlates with increased tumor malignancy and poor prognosis.[7] It was recently reported that c-Src plays important roles in neuroblastoma, which is the most common extracranial pediatric tumor.[8] Moreover, c-Src and other SFK members are involved in lymphomas and in leukemias, including chronic myeloid leukemia (CML).[9]

In the last few years, extensive efforts have been devoted to the identification of small molecules that are able to selectively target SFKs. The pyrazolopyrimidines PP1 and PP2 (Figure 1)[10] are the first reported SFK inhibitors. Initially, these compounds

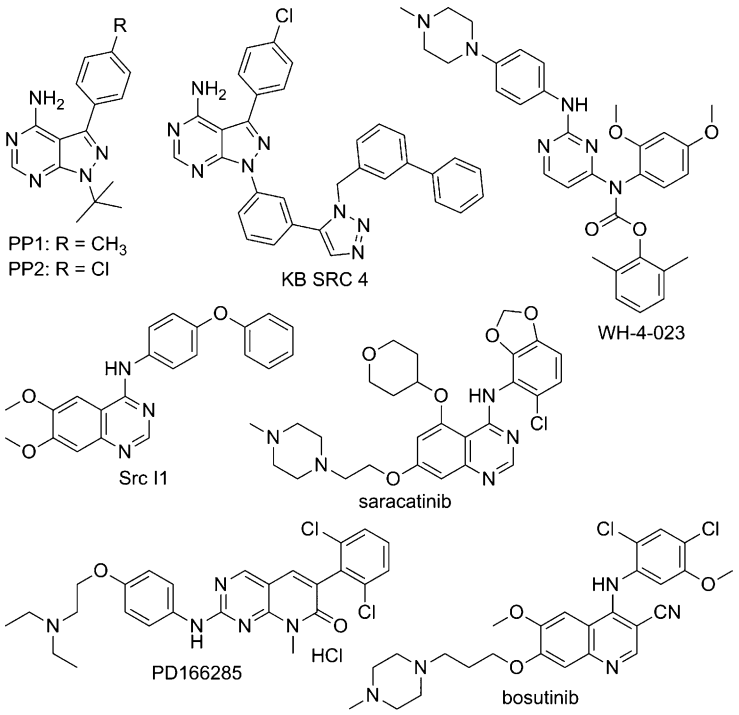

Figure 1. Structures of PP1 and PP2, KB SRC 4, Src I1, saracatinib, WH-4-023, PD166285, and bosutinib.

were found to be SFK-selective inhibitors in tests with a panel of 73 kinases,[11] but later a KINOMEscan analysis on 200 kinases indicated that PP2 is not selective for SFKs. Indeed, the compound showed activity on 56 kinases,[12] and a similar behavior is predicted for PP1.

Based on the co-crystal structure of PP2 bound to c-Src, Soellner and co-workers hypothesized that PP2 could be modified to obtain a selective SFK inhibitor, also endowed with c-Src selectivity.[12] Specifically, a pocket formed by the phosphate binding loop (P-loop, also known as the glycine-rich loop) was identified in c-Src. This pocket is not present in homologous kinases. Consequently, a series of PP2 analogues were synthesized and tested, leading to the identification of KB SRC 4 (Figure 1), which showed a K_d value of 86 nM for c-Src. Moreover, KB SRC 4 was demonstrated to be selective for c-Src among the other SFK members, with more than twofold selectivity over both Lck (160 nM) and Fgr (240 nM), eightfold selectivity over c-Yes (720 nM), and >40-fold selectivity over Lyn (3200 nM), Hck (4400 nM), and Fyn (>40000 nM).[12]

The quinazolines Src-I1[11] and saracatinib[13] (Figure 1), which are currently undergoing clinical trials for different tumors, are potent inhibitors of c-Src, with respective IC_{50} values of 180 and 27 nM, but they also inhibit other SFK members such as Lck and Yes. Over the years, other compounds have been studied for their selectivity against SFK members. They include WH4-0-23 (Figure 1), a potent and selective Lck and Src inhibitor (IC_{50} values of 2 and 6 nM, respectively),[14] PD166285, which showed a K_i value of 4.9 nM on c-Src,[15–17] and bosutinib (IC_{50}: 1.2 nM for c-Src; Figure 1).[18] However, it is important to consider that obtaining selectivity across this conserved kinase family is a very challenging task, with only a handful of compounds identified that can discriminate between them.

The most important SFK inhibitor is dasatinib (**1**; Figure 2), which has been approved for the treatment of Philadelphia+ (Ph+) CML and acute lymphoblastic leukemia (ALL). It is also in clinical trials for the treatment of non-Hodgkin's lymphoma, metastatic breast cancer, prostate cancer, and other tumors.[19] This compound also inhibits other TKs, including Bcr-Abl, Kit, PDGFR, ephrin A receptor kinase, and the Tec kinase Btk.[20] Regarding dasatinib's selectivity toward SFK members, a KINOMEscan analysis published in 2011 by Davis et al.[21] showed that dasatinib possesses K_d values of 0.21, 0.3, 0.53, and 0.79 nM toward c-Src, Yes, Lyn, and Fyn, respectively.

As has been widely reported, kinase inhibitors usually have heteroaromatic groups capable of interacting with the hinge region, which is located in the ATP binding pocket of the catalytic domain.[22] The hinge region is highly conserved in different kinase families.[23] The synthesis of new hinge-interacting functionalities is therefore crucial to obtain new molecules that may be selective for one or few kinases while being endowed with high inhibitory potency.

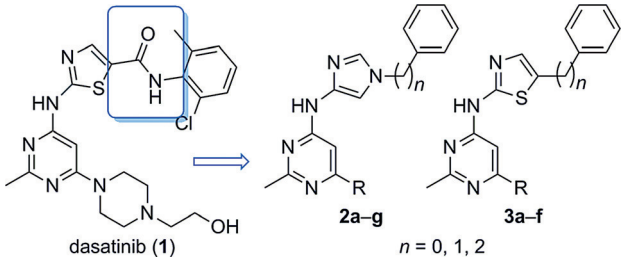

Figure 2. Replacement of the amidic linker of dasatinib to obtain compounds **2a–g** and **3a–f**.

This study is focused on the synthesis and biological evaluation of two series of compounds, active as SFKs inhibitors, bearing heterocyclic moieties that may interact with the hinge region. The 4-aminoimidazole ring of compounds **2a–g** was chosen for study because it is underexplored in the TK inhibitor literature. Researchers at AstraZeneca first investigated the ability of the 4-aminoimidazole moiety to bind the hinge of Jak2 kinase.[24] The authors compared the 4-aminoimidazole group with 5-aminopyrazole (a well-known hinge binder in kinases),[25] and they found that the 4-aminoimidazole ring could be an effective replacement for 5-aminopyrazole. Moreover, we inserted the 2-aminothiazole moiety, which is present in dasatinib, into compounds **3a–f**. Because dasatinib binds c-Src in the low-nanomolar range,[26,27] this is a good starting point for the investigation of other derivatives (Figure 2). The amide linker between the 2-aminothiazole moiety and the aromatic ring of dasatinib has been considered as a constraint in terms of exploring the distance between the hinge region and the

hydrophobic pocket. This region is occupied by the 2-chloro-6-methylbenzamide moiety of dasatinib, while its substituted pyrimidine occupies a hydrophobic cleft created by Leu273 and Gly344.[27] We decided to substitute the amidic linker between the heterocyclic ring (thiazole or imidazole) and the phenyl groups with alkyl chains (methyl or ethyl) or to remove it completely. The space around the hydrophobic pocket was therefore studied by using various linker lengths on the basis of structural simplicity and pliability.

Regarding the solubilizing side chain present on the pyrimidine ring, we initially decided to maintain the (2-hydroxyethyl)-piperazin-1-yl group of dasatinib. We then attached various N-linked amine, O-linked alcohol, and O-linked amine groups to the pyrimidine core to investigate the polarity and basicity necessary in the solvent-exposed area of c-Src kinase[28] (Table 1). The hits thus obtained were evaluated to identify promising c-Src inhibitors with good biological activity.

Results and Discussion

Chemistry

We first synthesized compounds **2a**–**g**, which belong to an underexplored chemical class, in order to verify the capacity of the 4-aminoimidazole ring to act as a hinge binder for c-Src. The commercially available 4-nitro-1*H*-imidazole **4** was regioselectively alkylated with selected alkylating agents to give intermediates **5a**–**c** in high purity and yield.[29] In particular, we used iodobenzene, copper(I) iodide, and L-proline to obtain compound **5a**, and (bromomethyl)benzene or (2-bromoethyl)-benzene to obtain compounds **5b** and **5c**, respectively.

Palladium-mediated hydrogenation of **5a**–**c** afforded the corresponding amino derivatives as free bases, which were immediately converted into hydrochloride salts, as the compounds are unstable as free bases, to yield derivatives **6a**–**c** (Scheme 1). At this point the next step of substitution was performed in two different ways based on the length of the scaffold previously synthesized.

In detail, compounds **6b**,**c** were regioselectively coupled with the commercially available 4,6-dichloro-2-methylpyrimi-

Table 1. Inhibitory activity of compounds **2a**–**g** and **3a**–**f**.

Scaffold	R	*n*	Compd	IC_{50} [μM] c-Src	Yes	Lyn	Fyn
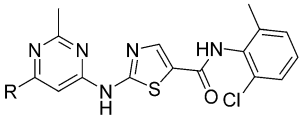	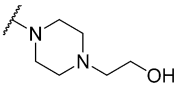		**1**	$<0.004^{[a]}$	$<0.009^{[a]}$	$<0.0009^{[a]}$	$<0.003^{[a]}$
	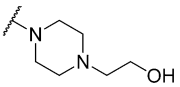	0	**2a**	$0.484\pm0.06^{[a]}$	NT	$0.335\pm0.02^{[a]}$	$1.3\pm0.2^{[b]}$
		1	**2b**	$2.0\pm0.13^{[b]}$	$2.0\pm0.08^{[b]}$	$\geq3^{[b]}$	NA[b]
		2	**2c**	$0.220\pm0.03^{[a]}$	$0.689\pm0.10^{[a]}$	$1.3\pm0.02^{[a]}$	$0.167\pm0.03^{[a]}$
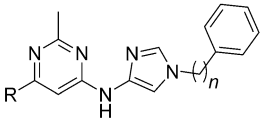	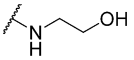	2	**2d**	$\geq3^{[b]}$	NT	$1.9\pm0.09^{[b]}$	NA[b]
	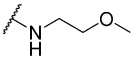	2	**2e**	$1.5\pm0.30^{[b]}$	NT	$\geq2^{[b]}$	NA[b]
	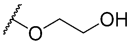	2	**2f**	$\geq3^{[b]}$	$\geq3^{[b]}$	$\geq3^{[b]}$	$0.641\pm0.10^{[a]}$
	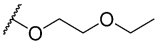	2	**2g**	$\geq3^{[b]}$	$\geq3^{[b]}$	$\geq3^{[b]}$	$0.659\pm0.03^{[a]}$
	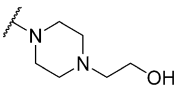	1	**3a**	$0.093\pm0.004^{[a]}$	$0.233\pm0.02^{[a]}$	$0.318\pm0.02^{[a]}$	$0.252\pm0.03^{[a]}$
		0	**3b**	$0.097\pm0.01^{[a]}$	$0.335\pm0.03^{[a]}$	$0.433\pm0.03^{[a]}$	$0.220\pm0.02^{[a]}$
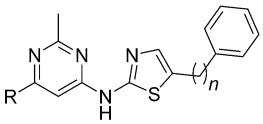	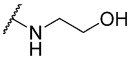	0	**3c**	$0.208\pm0.01^{[a]}$	NT	$0.474\pm0.05^{[a]}$	$\geq2^{[b]}$
	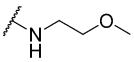	0	**3d**	$\geq2^{[b]}$	$\geq2^{[b]}$	$\geq2^{[b]}$	$0.661\pm0.25^{[a]}$
	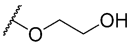	0	**3e**	$\geq2^{[b]}$	$\geq3^{[b]}$	$\geq2^{[b]}$	$1.6\pm0.3^{[b]}$
	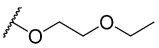	0	**3f**	$\geq3^{[b]}$	$\geq3^{[b]}$	$\geq3^{[b]}$	NA[b]

[a] The compound was tested in two independent experiments, and IC_{50} values are the mean ± SD. [b] The compound was tested in a single experiment. Dasatinib (**1**) was used as reference; the IC_{50} values of dasatinib were less than that of enzyme concentrations, which were 4, 9, 0.9, and 3 nM for Src, Fyn, Lyn A, and Yes 1, respectively (see Experimental Section for details).

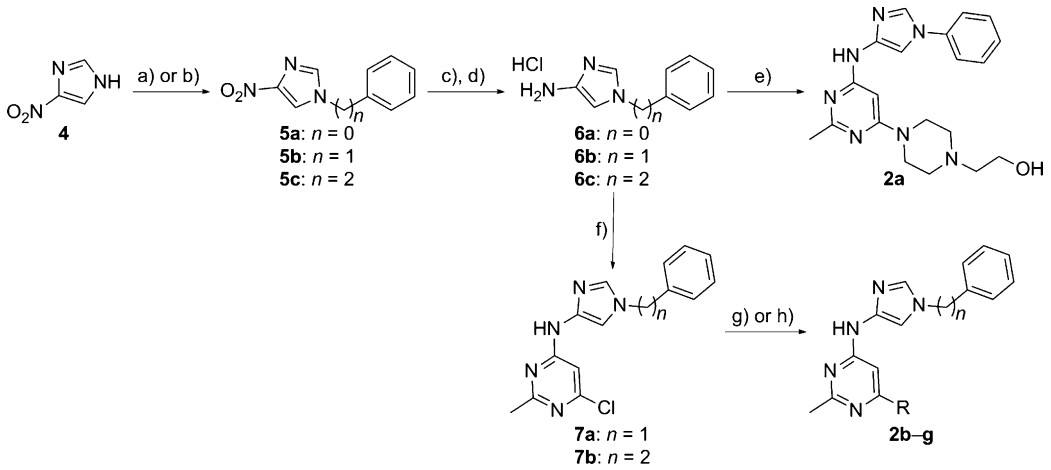

Scheme 1. *Reagents and conditions*: a) C_6H_5I, copper(I) iodide, L-(−)-proline, K_2CO_3, DMSO, 85 °C, overnight (for $n=0$); b) R-Br, K_2CO_3, CH_3CN, 60 °C, overnight (for $n=1$, 2); c) H_2, Pd/C, EtOH, 5 h, atmospheric pressure; d) HCl in EtOH (2 M), RT, 30 min; e) 2-(4-(6-chloro-2-methylpyrimidin-4-yl)piperazin-1-yl)ethanol **11**, Xantphos, Pd_2dba_3, $CsCO_3$, dioxane, 95 °C, overnight, then 110 °C for 2 h (for $n=0$); f) 4,6-dichloro-2-methylpyrimidine, DIPEA, DMSO, 50 °C, 5 h (for $n=1$, 2); g) R_2-NH, DIPEA, DMSO, 100 °C, overnight, or R-NH_2, diethylene glycol monomethyl ether, 130 °C, overnight; h) ethylene glycol or ethylene glycol monomethyl ether as solvent, NaH (60% dispersion in mineral oil), 130 °C, 2 h.

dine at 50 °C in the presence of DIPEA to afford intermediates **7a**,**b** (Scheme 1). Different amines and alcohols then replaced the chlorine atom on the pyrimidine core of the intermediates **7a**–**b**, leading to compounds **2b**–**g**. The R groups (Table 1) were chosen with the aim of creating molecules with reasonable solubility profiles.

On the other hand, reaction of **6a** with 2-(4-(6-chloro-2-methylpyrimidin-4-yl)piperazin-1-yl)ethanol **11** afforded compound **2a** (in which the phenyl ring is linked directly to the imidazole ring). The building block **11** was in turn prepared from dichloropyrimidine **12** and 2-(piperazin-1-yl)ethanol following a procedure used for dasatinib synthesis[30] as shown in Scheme 2.

In the second part of this work, thiazole derivatives of dasatinib were prepared. In these compounds the amide linker between the thiazole moiety and the aromatic ring of dasatinib is substituted by methylene unit (compound **3a**) or is removed altogether (compounds **3b**–**f**), in order to investigate the effects of these changes on biological activity. (Schemes 3 and 4).

The building block **10**, carrying a methylene linker between the thiazole and the aromatic ring, was synthesized following a procedure of thiazole synthesis reported by Miller et al.[31] The commercially available aldehyde **8** was converted into aminothiazole **10** by reaction with thiourea onto a non-isolated chloro derivative **9**. To obtain the first derivative of this class **3a**, intermediate **10** was coupled with compound **11** in a Buchwald reaction (Scheme 3).

Because the final step in the preparation of compound **3a** had a low yield, we preferred to move to the synthesis of

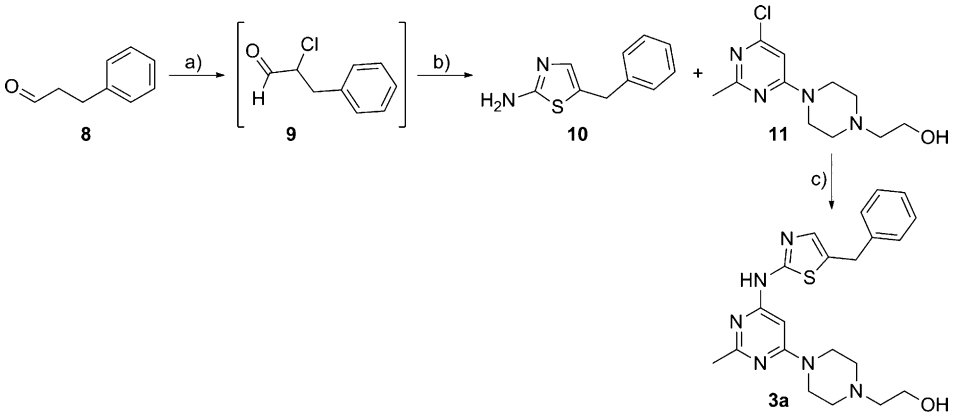

Scheme 3. *Reagents and conditions*: a) NCS, L-proline, CH_2Cl_2, 0 °C→RT, 12 h; b) thiourea, EtOH, reflux, 5 h; c) Xantphos, Pd_2dba_3, $CsCO_3$, dioxane, 100 °C, 4 h.

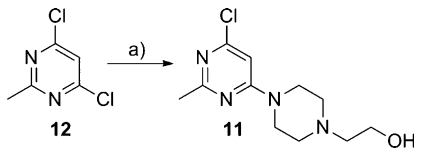

Scheme 2. *Reagents and conditions*: a) 2-(piperazin-1-yl)ethanol, triethylamine, CH_2Cl_2, 30 °C, overnight.

compounds **3b**–**f**, in which the thiazole moiety is directly linked to the phenyl ring. For the synthesis of these compounds, the commercially available 5-phenylthiazol-2-ylamine **13** was reacted with **12**. This led to intermediate **14**, common to the final compounds **3b**–**f**, which were obtained by reaction of **14** with the suitable amine or alcohol (Scheme 4).

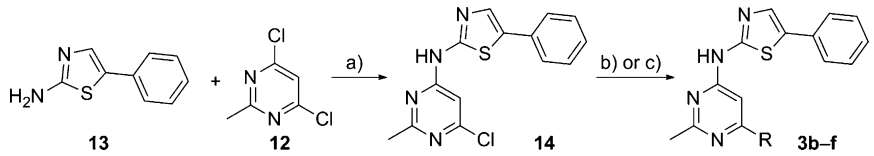

Scheme 4. *Reagents and conditions*: a) Xantphos, Pd_2dba_3, $CsCO_3$, dioxane, 95 °C, 12 h; b) R_2-NH, DIPEA, DMSO, 80 °C, overnight, or R-NH_2, diethylene glycol monomethyl ether, 100 °C, overnight; c) ethylene glycol or ethylene glycol monomethyl ether as solvent, NaH (60% suspension in mineral oil), 130 °C, 12 h.

To evaluate the biological responses, all final compound activities versus the target kinase were assayed within the Rottapharm in vitro screening department, using a Z′-LYTE technology kit.[32] Each compound was tested against four members of the Src family (c-Src, Yes, Lyn, and Fyn), and the inhibitory activities are expressed as IC_{50} values.

Enzyme activity data showed that the most interesting compounds are present in the thiazole series. Indeed, derivatives **3a** and **3b** inhibit c-Src with IC_{50} values of 93 and 97 nM, respectively. They are also active on Yes, Lyn, and Fyn, with IC_{50} values in the range of 220–433 nM. Derivative **3c** is slightly less active than **3a** and **3b** on Src, possessing an IC_{50} value of 208 nM. All thiazole derivatives, however, show lower inhibitory potency than dasatinib, indicating that replacement of the amidic chain of dasatinib results in a loss—even if acceptable—of activity.

Among the aminoimidazole series (compounds **2a**–**g**), derivatives **2a** and **2c** also show a certain amount of inhibitory activity toward c-Src, with respective IC_{50} values of 484 and 220 nM. This suggests that the 4-aminoimidazole scaffold, properly functionalized, could be a viable replacement for 2-aminothiazole. In both series, the R group conferring the best inhibitory profile is the (2-hydroxyethyl)-1-piperazinyl group, present in dasatinib.

Molecular modeling

c-Src is one of the few thoroughly characterized and well-validated targets in anticancer therapy, and its three-dimensional structure is well known (Figure 3).[33–36] Molecular docking simulations have been performed to hypothesize the way by which the new synthesized inhibitors bind c-Src and to gain insight on the peculiar chemical features that influence their activity toward the isolated enzyme (Table 1). To achieve this goal within a reasonable timeframe, we required a rapid and robust docking tool.

Docking studies were performed by using Glide[37,38] software. The reliability of the docking protocol was first checked by simulation of the interactions between dasatinib and c-Src and comparison of the modeled complexes with the experimental structures. In detail, the X-ray crystal structure of c-Src in complex with dasatinib was retrieved from the RCSB Protein Data Bank (PDB ID: 3G5D).[39] Dasatinib was removed from the crystal structure, and the protein was prepared for the docking procedure by using the Protein Preparation Wizard[40] protocol implemented in Maestro.[41] The inhibitor was drawn, minimized, and finally docked in the ATP binding site of 3G5D. As a result, the program perfectly reproduced the experimental binding mode of dasatinib, as demonstrated by the low root-mean-square deviation (RMSD) of 0.45 Å (calculated on all the ligand heavy atoms; Figure 4). The docking score found for dasatinib was −11.434 kcal mol^{-1}.

Dasatinib adopted an extended conformation within the ATP binding site of c-Src with the formation of three hydrogen bonds. A pair of hydrogen bonds was found in the hinge region of the ATP binding site: between the N3 acceptor of the aminothiazole ring of dasatinib and the NH donor of Met341, and between the 4-NH donor of dasatinib and the carbonyl oxygen acceptor of Met341. The third hydrogen bond was formed between the side chain oxygen atom of Thr338 gatekeeper and the amide moiety of the ligand (Figure 4). Moreover, dasatinib participated in two heteroaromatic CH–O=C interactions with the hinge region backbone and in other contacts that are mainly mediated by van der Waals interac-

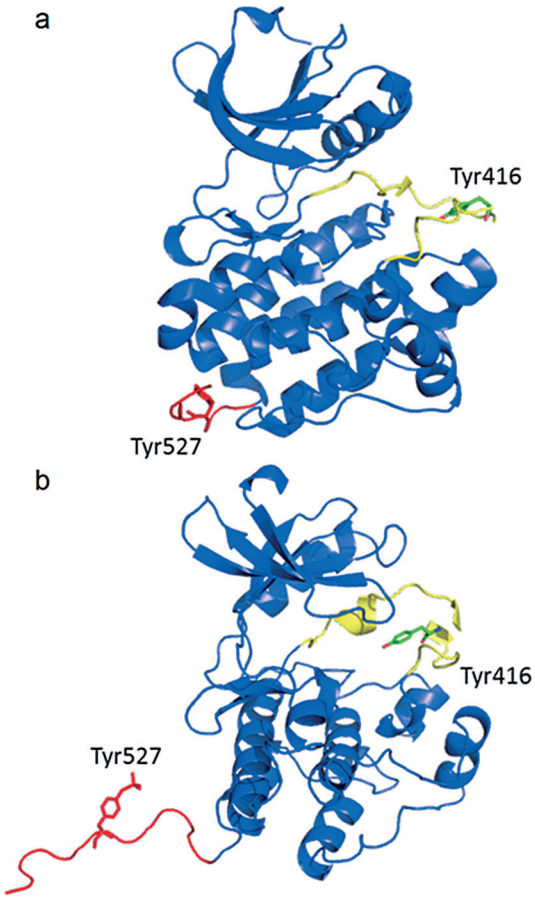

Figure 3. a) Reassembled active-like conformation of c-Src kinase, showing the kinase domain in blue, the activation loop (yellow) with its Tyr416 residue in green, and the C-terminal tail that contains non-phosphorylated Tyr527 (red). b) Auto-inhibited conformation of c-Src kinase, in which Tyr527 is phosphorylated (the coloring scheme is the same as in panel a).

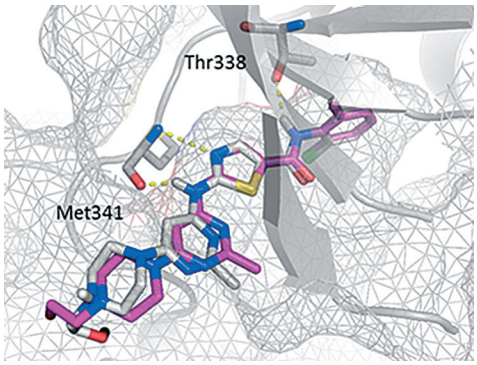

Figure 4. Docking pose of dasatinib (gray structure) in the ATP binding site of c-Src. The X-ray structure is overlaid for reference (magenta). For clarity, only a few active site residues are shown (gray). Hydrogen bonds are shown as yellow dashes.

tions. Once the reliability of the docking procedure was tested, the interaction pathway between inhibitors and Src was simulated by applying the same protocol used for dasatinib.

All the aminothiazole and aminoimidazole derivatives were docked within the ATP binding site of c-Src. Simulations allowed for the identification of two different binding modes related to the R substituent on the pyrimidine group. Compounds **3a**–**f**, belonging to the aminothiazole family, showed an interaction pathway similar to that previously found for dasatinib with the first binding pose which overlapped the crystallographic ligand (Figure 5a). In the first docking pose, the thiazole moiety occupies the same position as in dasatinib, and the phenylethylene linker establishes contacts with the hydrophobic region I (HRI) interacting with Thr338, Lys295, Val281, Met314, Val323, Ala293, and Phe405. Two hydrogen

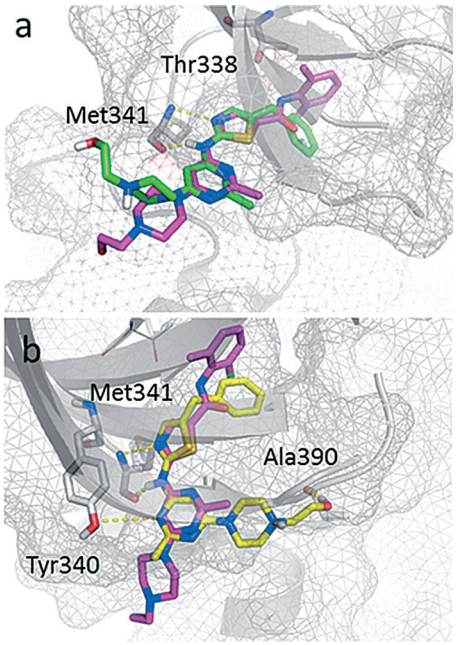

Figure 5. Superimposition of the a) first (green) and b) second (yellow) docking poses of compound **3a** onto the X-ray crystal structure of dasatinib (magenta). Hydrogen bonds are shown as yellow dashes.

bonds were also found with Met341. Because of the absence of the amide group in the spacer of **3a**–**f**, no hydrogen bonds were observed with Thr338. Furthermore, the R substituent on the pyrimidine ring projected into the solvent-accessible area, perfectly reproducing the experimental pose of dasatinib. In the alternate binding mode, the pyrimidine ring was rotated 180°, with the methyl substituent directed toward the hinge region, and the R group involved in electrostatic interactions with Asp348, Ala390, Cys345, and Tyr340 (Figure 5b). In accordance with the experimental evidence, higher docking scores were obtained for compounds **3a**–**c** in the series of thiazoles. In contrast, compounds **3d**–**f**, which present a small and very flexible R group on the pyrimidine ring, were not allowed to stabilize their binding to the enzyme.

Docking studies on compounds **2a**–**g**, endowed with an aminoimidazole hinge binder, gave the binding mode shown in Figure 6. In detail, the nitrogen atom at the 3-position acted as a hydrogen bond acceptor in the interaction with Met341,

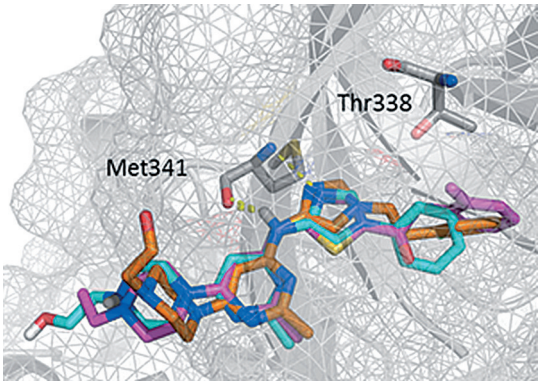

Figure 6. Compounds **2a** (cyan) and **2c** (orange) docked into the ATP binding site of c-Src. The X-ray structure of dasatinib (magenta) is shown as reference. For clarity, only residues involved in the most important interactions are highlighted. Hydrogen bonds are shown as yellow dashes. Met341 is the common residue of the hinge with which all three structures form a hydrogen bond.

while the exocyclic piperazine of the most active compounds (**2a** and **2c**) was solvent exposed. The phenyl group kept contacts with residues of the HRI through van der Waals interactions. Interestingly, the phenyl group of compound **2c** perfectly overlapped the 2-chloro-6-methylphenyl moiety of dasatinib. On the other hand, compound **2a** did not completely fill the HRI because of the absence of a linker long enough to enable the phenyl ring to deeply interact with the hydrophobic pocket. In agreement with in vitro data ($IC_{50} = 0.4\ \mu M$), compound **2a** has a smaller docking score ($\Delta G_{bind} = -9.097$ kcal mol^{-1}) than its analogue **2c** ($\Delta G_{bind} = -10.028$ kcal mol^{-1}).

In conclusion, molecular docking studies allowed us to identify a possible and rational binding mode for synthesized compounds within the ATP binding site of c-Src. Furthermore, it was demonstrated that the imidazole ring could replace the thiazole moiety, being able to establish the same crucial contacts with the most important residues belong to the hinge region.

Homology modeling

The results of the primary set of compounds tested in vitro (Table 1) displayed a different activity among Src family members tested (Src, Fyn, Yes, and Lyn). Compounds **3a**–**c** showed certain selectivity, being twofold more selective for c-Src with respect to the other three kinases. With the aim of explaining the differences in terms of enzyme inhibitory activity, all compounds were docked within the ATP binding site of Fyn, Yes, and Lyn. To obtain comparable results and to avoid differences in protein conformations derived from adaptation to the co-crystallized ligands, the X-ray structures of the Src family members in complex with dasatinib were retrieved from the PDB. In particular, the structure of PDB ID 2ZVA[42] was used to assess the docking protocol on Lyn kinase. On the other hand, no structures were found for Yes in the PDB, and only one X-ray crystal structure of Fyn in complex with staurosporine (PDB ID: 2DQ7)[43] was available.

A homology modeling approach[44,45] (see Experimental Section below for details) was then applied by using the crystal structure of the human c-Src catalytic domain in complex with dasatinib, and the FASTA sequences of Fyn and Yes as query. The sequence identity between the kinase domains of Fyn and Yes versus Src was ~70%. The homology models were constructed by including residues 257–533 as shown in Figure 7. The derived protein structures were minimized and then used as the starting point for docking simulations. Compounds **3a**–**f** and **2a**–**g** were all docked together with dasatinib, used as standard, to assess the protocol. As expected, docking poses of dasatinib obtained in all the 3D structures reproduced the experimental binding mode observed in c-Src, showing the same two points of interaction with Met341 and Thr338 in all kinases.

For all three kinases, an overall agreement was found between the docking scores and their enzymatic activities. Furthermore, the contribution to binding was calculated for each residue belonging to the active site. Eight amino acids were found to be dissimilar between Fyn kinase and c-Src, both in energy and in residue type. These differences were not so discriminating for the binding mode. On the other hand, Tyr340 in the c-Src sequence was found to be substituted in Yes and Lyn, with a Phe at positions 340 and 321, respectively. This mutation had significant consequences in our docking simulations: the OH group of the tyrosine residue on c-Src was able to contact the solvent-exposed side chain of the ligands, creating coulombic interactions that are absent in Yes and Lyn due to the lack of this polar group (Figure 8). This feature could partially explain the higher potency of **3b** against c-Src rather than Lyn and Yes.

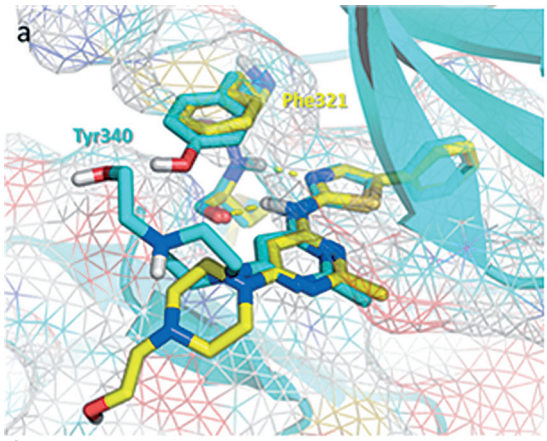

b

Protein	Position	Residue	ΔG_{bind} [kcal mol^{-1}]
Src	340	Tyr	–11.780
Lyn	321	Phe	–4.408
Yes	340	Phe	–4.215

Figure 8. a) Binding mode of compound **3b** docked to Yes (yellow) and c-Src (cyan). b) Binding free energies (ΔG_{bind}) of Tyr340 at c-Src and Phe340 and Phe321 at Yes and Lyn, respectively.

Molecular dynamics

To assess the stability of the complexes and to gain further insight into the ligand–protein interactions, molecular dynamics (MD) simulations were carried out by starting from the geometry obtained by docking. Four compounds (dasatinib, **2c**, **2g**, and **3b**) in complex with c-Src were selected. Each simulation was carried out for a total of 50 ns. Figure 9 shows the time evolution of the RMSD calculated on all heavy atoms during the time of simulation with respect to the starting structures. For each analyzed complex we observed an initial increase due to equilibration of the system, followed by stabilization of the RMSD values. The most RMSD-stable regions of all simulations were regarded as stable and used to extract 200 evenly distributed snapshots from each trajectory.

Molecular mechanics Poisson–Boltzmann/generalized Born surface area (MM-GBSA) approaches were then applied to estimate the free energy of binding between protein and ligands. The computed values are listed in Table 2. A better correlation

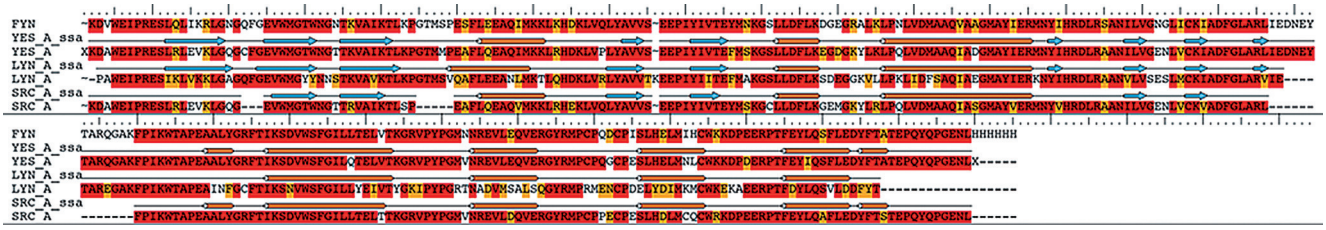

Figure 7. Sequence alignment of Fyn, Yes, Lyn, and Src. Residues that are uniquely conserved in the Src family are highlighted in red. The α-helices are represented with red cylinders, β-strands as cyan arrows, and loops as black lines.

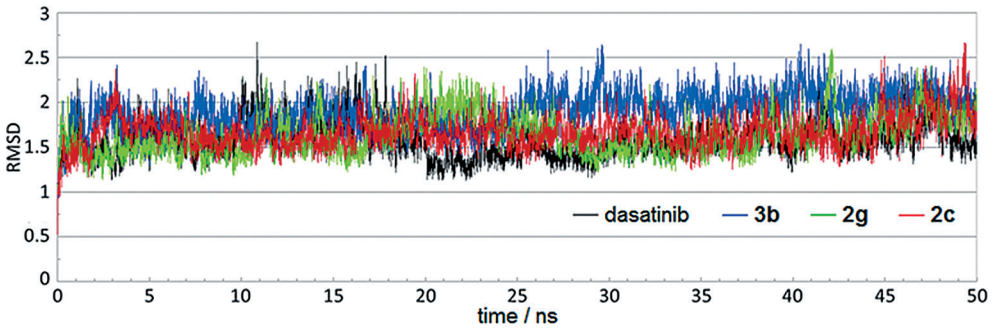

Figure 9. Time evolution of RMSD values (calculated on α-carbon atoms) of all complexes analyzed by MD simulations: dasatinib (black), **3b** (blue), **2g** (green), and **2c** (red).

Table 2. Binding free energies calculated by MM-GBSA for the ligands under study.

Compd	ΔG_{bind} [kcal mol^{-1}]
dasatinib	−51.92
3b	−44.37
2g	−32.42
2c	−42.53

between the computed binding free energies and inhibitory activities of the selected compounds was observed (Table 2). Indeed, the most potent compound in the enzyme assay showed the lower free binding energy value, whereas the inactive compound **2g** displayed the higher one. Residue decompositions were also analyzed and are summarized in Table 3. Compounds **2c** and **3b** showed the same residue profile as that of dasatinib. Interestingly, Thr338 interacts with both dasatinib and compound **2c** in two different ways. The amidic linker on dasatinib engages in a hydrogen bond with Thr338 ($\Delta G_{ele} = -1.26$ kcal mol^{-1}), whereas compound **2c** establishes only van der Waals interactions with the same residue ($\Delta G_{vdW} = -1.28$ kcal mol^{-1}). Crucial interactions with Val283 and Thr338 emerged as a hot spot for the ligand–protein binding stabilization of dasatinib and the most active compound in the aminoimidazole series **2c**.

Table 3. Hot spots in ligand–protein interaction identified for all simulations.[a]

Residue	Total ΔG_{bind} [kcal mol^{-1}]			
	dasatinib	**2c**	**2g**	**3b**
Leu273	−2.45	−2.35	−2.93	−2.22
Val281	−1.26	−1.87	−1.17	−1.52
Lys295	–	–	–	−1.14
Val323	−1.06	−1.05	–	–
Thr338	−2.81	−1.36	–	–
Tyr340	−2.49	−3.01	−3.22	−2.82
Met341	−3.36	−3.07	−3.21	−3.26
Gly344	−1.33	−1.06	−1.40	−1.38
Leu393	−2.10	−2.04	−1.96	−1.68

[a] Only residues with an energy less than −1 kcal mol^{-1} are reported.

Cell-based assays

With the aim of getting further insight into the biological profile of the synthesized compounds, the biological effect of **2a**, **2c**, **3a**, **3b**, and **3c** was evaluated on two human tumor cell lines: the neuroblastoma cell line SH-SY5Y, and the leukemia cell line K562, which have been previously described as being dependent on SFKs for their proliferation.[46,47] Dasatinib was also tested as reference compound. Cell lines were treated with various dilutions of the compounds, and cell viability and proliferation was measured by counting viable cells after 72 h of incubation (Figure 10). Compound **3b** was not tested at 10 μM, citing solubility problems. The compounds effected dose-dependent inhibition of cell proliferation in both cell lines, with the best antiproliferative profile associated with **3b**, which showed IC_{50} values of 3.6 and 0.5 μM on SH-SY5Y and on K562 cell lines, respectively.

The antitumor effect of **3b** was also evaluated by cell-cycle analysis (Figure 11). SH-SY5Y and K562 cells were treated with increasing concentrations of the compound (0.01–1 μM), and the percentage of cells in each phase of the cell cycle was

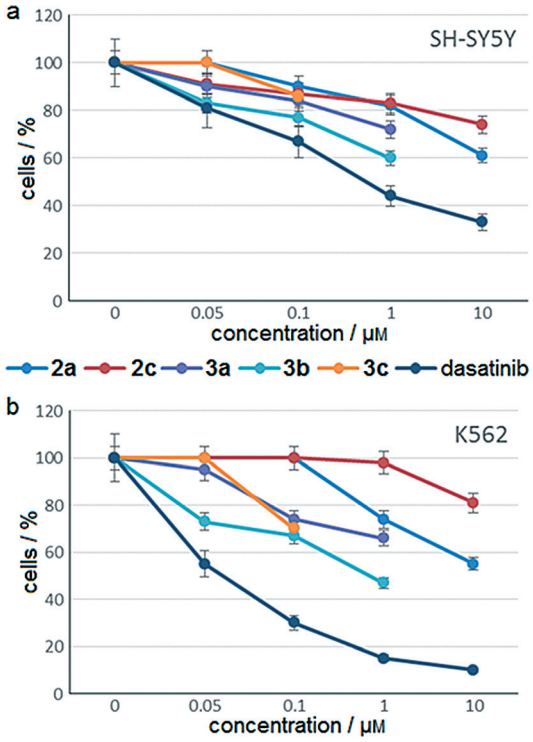

Figure 10. Proliferation analyses of a) SH-SY5Y and b) K562 cells were performed in the presence of **2a**, **2c**, **3a**, **3b**, **3c**, and dasatinib (reference compound) at increasing concentrations. The number of vital cells was measured after culture for 72 h. Values are the mean ± SD of three independent experiments.

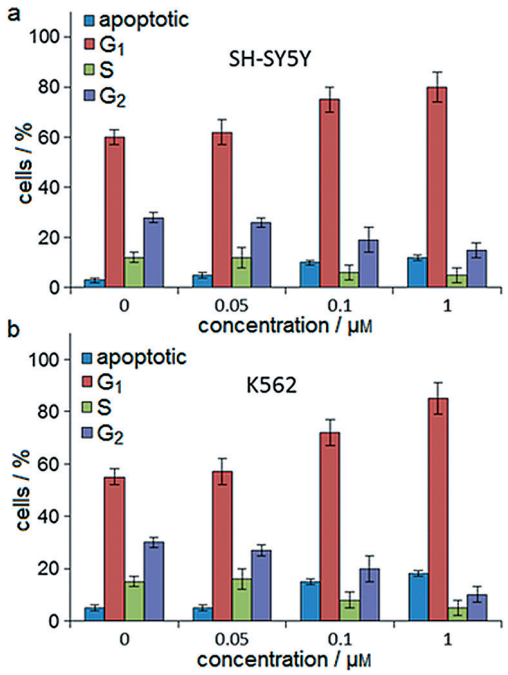

Figure 11. Analysis of the cell-cycle distribution of a) SH-SY5Y and b) K562 cells after treatment with increasing concentrations of **3b**. The cell-cycle status was investigated by cytofluorimetric analysis of DNA content, and results are expressed as a percentage of cells in each phase of the cell cycle with respect to total viable cells. Apoptosis was evaluated by determining the number of hypodiploid cells, and is expressed as the percentage of apoptotic cells with respect to total (viable and dead) cells. Results are the mean ± SD of three independent experiments; $*p < 0.01$ with respect to the value of untreated cells.

evaluated by cytofluorimetric analysis of DNA content. Compound **3b** caused a significant and dose-dependent accumulation of both cell lines in the G_1 phase, starting from 0.1 μM. In parallel we observed a significant accumulation of apoptotic cells only for the K562 line at higher concentrations of **3b**.

As expected, cell-based assay data reflect the behavior observed in enzyme-based tests. Dasatinib consistently showed higher antiproliferative activity than that of our compounds toward both SH-SY5Y and K562 cell lines. However, the difference in activity between **3b** and dasatinib at 1 μM on SH-SY5Y cells is lower than that on with K562 cells at the same concentration. This can be explained by the expression of the Bcr-Abl TK in these cells which is potently inhibited by dasatinib.

Conclusions

This study is focused on the identification and synthesis of two series of compounds which are active as c-Src inhibitors and which bear heterocyclic moieties (the 4-aminoimidazole and 2-aminothiazole rings), which may interact with the c-Src hinge region. In vitro evaluation against recombinant c-Src showed the inhibitory activity of five hits identified in this work, and highlighted the possibility of using the 4-aminoimidazole ring as a new hinge binder for Src kinase. In vitro assays performed on two cancer cell lines confirmed a significant antiproliferative activity for representative compounds. In addition, the modeling studies identify a possible and rational binding mode of synthesized compounds within the ATP binding site of c-Src. Hot spots were also identified in our compounds, which could partially explain the different activities observed on various SFK members. Furthermore, it was demonstrated that the imidazole core could establish the same crucial contacts as the thiazole core, with the most important residues belonging to the hinge region. This suggests that the aminoimidazole scaffold, properly functionalized, is a good replacement for the aminothiazole scaffold. To conclude, these findings warrant further investigation of aminoimidazoles in more advanced studies to fully understand their potential as effective anticancer agents.

Experimental Section

Chemistry

Reagents used in the following examples were commercially available from various suppliers (e.g., Sigma–Aldrich, Fluorochem, Apollo Scientific) and were used without further purification. Anhydrous solvents over molecular sieves were used where indicated. Anhydrous reactions were run under a positive pressure of dry N_2. ^{1}H NMR spectra were recorded on a Bruker 400 MHz NMR spectrometer using [D_6]DMSO or $CDCl_3$. Chemical shifts (δ) are reported in ppm using residual solvent as internal standard. Splitting patterns describe apparent multiplicities and are designated as s (singlet), d (doublet), dd (doublet of doublets), ddd (doublet of doublet doublets), t (triplet), q (quartet), m (multiplet), and br s (broad singlet). IR spectra were recorded on a PerkinElmer Spectrum 100 FT-IR spectrometer. Mass spectra were acquired on an Ion Trap Thermo LCQ classic spectrometer, operating in positive (ES+) and negative (ES−) ionization modes. UPLC was performed on a Waters Acquity UPLC-SQD instrument using an Acquity UPLC-BEH C_{18} column (1.7 μM, 50×2.1 mm) eluting with a gradient of H_2O/HCOOH (0.1%)→CH_3CN/HCOOH (0.1%) or 10 mM $(NH_4)HCO_3$ (pH 9) and CH_3CN. Flash silica gel chromatography was performed on Biotage automatic flash chromatography systems (Isolera or SP1) using Biotage SNAP HP silica cartridges or Biotage SNAP KP-NH cartridges. Reversed-phase chromatography was performed on a Biotage automatic flash chromatography system (Isolera) using Redisep Gold C_{18}Aq cartridges. Reactions were monitored by thin-layer chromatography on 0.25 mm E. Merck silica gel plates (60 F_{254}), visualized with UV light. Melting points (mp) were determined with a Büchi B-540 apparatus. The following abbreviations are used herein: AcOH: acetic acid; CV: column volume; CyHex: cyclohexane; DIPEA: *N*,*N*-diisopropylethylamine; DMSO: dimethyl sulfoxide; EtOAc: ethyl acetate; EtOH: ethanol; MeOH: methanol; NCS: *N*-chlorosuccinimide; RT: room temperature.

4-Nitro-1-phenyl-1*H*-imidazole (5a): A solution of 4-nitro-1*H*-imidazole (400 mg, 3.54 mmol), C_6H_5I (722 mg, 3.54 mmol), K_2CO_3 (978 mg, 7.07 mmol), copper(I) iodide (101 mg, 0.531 mmol), and L-(−)-proline (61.1 mg, 0.53 mmol) in dry DMSO (2.5 mL) was heated at 85 °C overnight. The mixture was diluted with EtOAc (20 mL), and the solids were filtered out. The filtrate was washed with brine, dried over Na_2SO_4 and concentrated under vacuum. The crude was dissolved in a minimal volume of DMSO and acidified with AcOH (1 mL). The resulting solution was loaded onto a RediSep C_{18}Aq (50 g) column primed with H_2O + 0.1% AcOH. The column was then eluted with 2 CV of H_2O + 0.1% AcOH and then the eluent was gradually changed to CH_3CN + 0.1% AcOH over

10 CV. The fractions containing the desired product were pooled and stripped of solvent under vacuum to provide, on drying under high vacuum, a yellow solid (**5a**, 288 mg, 43%); mp: 95 °C. ^{1}H NMR (400 MHz, [D$_6$]DMSO): δ = 7.51 (d, J = 7.34 Hz, 1H), 7.55–7.64 (m, 2H), 7.81 (d, J = 7.83 Hz, 2H), 8.48 (d, J = 1.47 Hz, 1H), 9.00 ppm (d, J = 1.47 Hz, 1H); IR: $\tilde{\nu}$ = 1375 cm^{-1} (NO); MS (ESI+) m/z: 190.1 [M+H]$^+$ ($C_9H_7N_3O_2$).

General procedure for the preparation of intermediates 5b–c: Corresponding alkylating agents (commercially available; 1.1 mmol) were added to a solution of 4-nitro-1*H*-imidazole (5 g, 44.2 mmol) in CH_3CN (50 mL) and K_2CO_3 (9.17 g, 66.3 mmol). The resulting mixture was heated at 60 °C overnight. The reaction mixture was then filtered, and the filtrate was concentrated under vacuum, leaving a yellow solid. The desired product was recovered from this residue by normal-phase column chromatography on a Cartridge Biotage HP-SiO_2 (100 g) column primed with CH_2Cl_2 only. The column was then run for 4 CV with CH_2Cl_2 and then changed to CH_2Cl_2/MeOH 9:1 over 5 CV.

1-Benzyl-4-nitro-1*H*-imidazole (5b): 1-Benzyl-4-nitro-1*H*-imidazole **5b** was prepared starting from (bromomethyl)benzene (5.79 mL, 44.60 mmol). Pale-yellow solid (5 g, 55.6%); mp: 103 °C. ^{1}H NMR (400 MHz, [D$_6$]DMSO): δ = 5.31 (s, 2H), 7.31–7.46 (m, 5H), 8.00 (s, 1H), 8.48 ppm (d, J = 1.47 Hz, 1H); IR: $\tilde{\nu}$ = 1370 cm^{-1} (NO); MS (ESI+) m/z: 204.1 [M+H]$^+$ ($C_{10}H_9N_3O_2$).

4-Nitro-1-phenethyl-1*H*-imidazole (5c): 4-Nitro-1-phenethyl-1*H*-imidazole **5c** was prepared starting from (2-bromoethyl)benzene (7.27 mL, 53.1 mmol). Yellow solid (7.87 g, 82%); mp: 99 °C. ^{1}H NMR (400 MHz, [D$_6$]DMSO): δ = 3.12 (t, J = 7.34 Hz, 2H), 4.34 (t, J = 7.34 Hz, 2H), 7.16–7.26 (m, 3H), 7.26–7.34 (m, 2H), 7.74 (d, J = 0.98 Hz, 1H), 8.38 ppm (d, J = 1.47 Hz, 1H); IR: $\tilde{\nu}$ = 1365 cm^{-1} (NO); MS (ESI+) m/z: 218.1 [M+H]$^+$ ($C_{11}H_{11}N_3O_2$).

General procedure for the preparation of intermediates 6a–c: Intermediates described above (**5a–c**) were dissolved in EtOH and Pd/C was added. The mixture was subjected to hydrogenation at atmospheric pressure for 5 h at RT. The mixture was filtered to remove the catalyst, and then an excess of 1.25 M HCl in EtOH was added. The resulting solution was stirred for 30 min and concentrated under reduced pressure to give compounds **6a–c**.

1-Phenyl-1*H*-imidazol-4-amine hydrochloride salt (6a): 1-Phenyl-1*H*-imidazol-4-amine hydrochloride salt **6c** was prepared starting from 4-nitro-1-phenyl-1*H*-imidazole **5a** (288 mg, 1.52 mmol) and Pd/C (10 wt%, 68 mg, 0.064 mmol) providing a white solid (232 mg, 78%); mp: 98 °C. The compound appeared unstable as a salt as well, and so NMR and MS data were acquired immediately after synthesis. ^{1}H NMR (400 MHz, [D$_6$]DMSO): δ = 7.27 (br s, 1H), 7.48–7.54 (m, 1H), 7.57–7.63 (m, 2H), 7.73 (d, J = 7.83 Hz, 2H), 8.90 ppm (br s, 1H), (2H under solvent peak); MS (ESI+) m/z: 160.1 [M+H]$^+$ ($C_9H_{10}ClN_3$).

1-Benzyl-1*H*-imidazol-4-amine hydrochloride salt (6b): 1-Benzyl-1*H*-imidazol-4-amine hydrochloride salt **6b** was prepared from 1-benzyl-4-nitro-1*H*-imidazole **5b** (2.82 g, 13.88 mmol) and Pd/C (5 wt%, 1.24 g, 0.58 mmol), providing a yellow solid (2.56 g, 88%); mp: 167 °C (dec.). ^{1}H NMR (400 MHz, [D$_6$]DMSO): δ = 5.26 (s, 2H), 6.62 (d, J = 1.96 Hz, 1H), 7.32–7.44 (m, 5H), 8.65 ppm (d, J = 1.47 Hz, 1H), (2H under solvent peak); MS (ESI+) m/z: 174.1 [M+H]$^+$ ($C_{10}H_{12}ClN_3$).

1-Phenethyl-1*H*-imidazol-4-amine hydrochloride salt (6c): 1-Phenethyl-1*H*-imidazol-4-amine hydrochloride salt **6c** was prepared starting from 4-nitro-1-phenethyl-1*H*-imidazole **5c** (6.26 g, 28.80 mmol) and Pd/C (5 wt%, 2.58 g, 1.21 mmol), providing a yellow solid (6 g, 93%); mp: 148 °C (dec.). ^{1}H NMR (400 MHz, [D$_6$]DMSO): δ = 3.08 (t, J = 7.34 Hz, 2H), 4.28 (t, J = 7.09 Hz, 2H), 6.66 (d, J = 1.96 Hz, 1H), 7.19–7.34 (m, 5H), 8.34 ppm (d, J = 1.47 Hz, 1H), (2H under solvent peak); MS (ESI+) m/z: 188.1 [M+H]$^+$ ($C_{11}H_{14}ClN_3$).

***N*-(1-Benzyl-1*H*-imidazol-4-yl)-6-chloro-2-methylpyrimidin-4-amine (7a)**: 1-Benzyl-1*H*-imidazol-4-amine hydrochloride salt **6b** (150 mg, 0.71 mmol) was dissolved in dry DMSO (2.5 mL). 4,6-Dichloro-2-methylpyrimidine (128 mg, 0.79 mmol) and DIPEA (0.498 mL, 2.86 mmol) were added, and the mixture was heated at 50 °C for 5 h. Once the reaction was determined to be complete, DIPEA was evaporated, AcOH (0.5 mL) was added, and the resulting solution was loaded onto a RediSep C_{18}Aq column (50 g) column primed with H_2O + 0.1% AcOH. The column was then eluted with 2 CV of H_2O + 0.1% AcOH and then the eluent was gradually changed to CH_3CN + 0.1% AcOH over 10 CV. The fractions were then combined and evaporated to obtain an orange solid. This solid was then loaded onto a Cartridge Biotage KP-SiO2 column (25 g) primed with CyHex/EtOAc 1:1. The column was then run for 2 CV with CyHex/EtOAc 1:1 and then changed to EtOAc only over 6 CV. The fractions containing the desired product were pooled and stripped of solvent under vacuum to provide, upon drying under high vacuum, a pale-yellow solid. *N*-(1-*b*enzyl-1*H*-imidazol-4-yl)-6-chloro-2-methylpyrimidin-4-amine (**7a**) (64 mg, 30%); mp: 170–172 °C; ^{1}H NMR (400 MHz, [D$_6$]DMSO): δ = 2.40 (s, 3H), 5.20 (s, 2H), 6.57–6.86 (m, 1H), 7.26–7.42 (m, 6H), 7.64 (s, 1H), 9.92–10.21 ppm (m, 1H); IR: $\tilde{\nu}$ = 3260 cm^{-1} (NH); MS (ESI+) m/z: 300.1 [M+H]$^+$ ($C_{15}H_{14}ClN_5$).

6-Chloro-2-methyl-*N*-(1-phenethyl-1*H*-imidazol-4-yl)pyrimidin-4-amine (7b): To 1-phenethyl-1*H*-imidazol-4-amine hydrochloride salt **6c** (150 mg, 0.67 mmol) in dry DMSO (2.5 mL) 4,6-dichloro-2-methylpyrimidine (120 mg, 0.74 mmol) and DIPEA (0.467 mL, 2.68 mmol) were added. The reaction was heated at 50 °C for 3 h. Once the reaction was determined to be complete, DIPEA was evaporated, AcOH (0.5 mL) was added and the resulting solution was loaded onto a RediSep C_{18}Aq column (50 g) column primed with H_2O + 0.1% AcOH. The column was then eluted with 2 CV of H_2O + 0.1% AcOH and then the eluent was gradually changed to CH_3CN + 0.1% AcOH over 10 CV. The fractions were then combined and evaporated to obtain an orange solid. This solid was then loaded onto a Cartridge Biotage KP-SiO_2 column (25 g) primed with CyHex/EtOAc 1:1. The column was then run for 2 CV with CyHex/EtOAc 1:1 and then changed to EtOAc only over 6 CV. On pooling and removal of solvent under vacuum, a pale-yellow solid was recovered. 6-Chloro-2-methyl-*N*-(1-phenethyl-1*H*-imidazol-4-yl)pyrimidin-4-amine **7b** (57 mg, 27%); mp: 161–163 °C; ^{1}H NMR (400 MHz, [D$_6$]DMSO): δ = 2.43 (s, 3H), 3.05 (t, J = 7.09 Hz, 2H), 4.22 (t, J = 7.34 Hz, 2H), 6.56–6.84 (m, 1H), 7.19–7.33 (m, 6H), 7.35–7.39 (m, 1H), 9.87–10.10 ppm (m, 1H); IR: $\tilde{\nu}$ = 3262 cm^{-1} (NH); MS (ESI+) m/z: 314.1 [M+H]$^+$ ($C_{16}H_{16}ClN_5$).

2-(4-(2-Methyl-6-((1-phenyl-1*H*-imidazol-4-yl)amino)pyrimidin-4-yl)piperazin-1-yl)ethanol (2a): To 4,5-Bis(diphenylphosphino)-9,9-dimethylxanthene (29.6 mg, 0.051 mmol), tris(dibenzylideneacetone)dipalladium (14.04 mg, 0.015 mmol), 1-phenyl-1*H*-imidazol-4-amine hydrochloride salt **6a** (100 mg, 0.51 mmol) and 2-(4-(6-chloro-2-methylpyrimidin-4-yl)piperazin-1-yl)ethanol **11** (144 mg, 0.56 mmol) was added dry dioxane (5 mL). The mixture was evacuated and backfilled with N_2 (this sequence was carried out a total of three times). The reaction was heated at 95 °C overnight and at 110 °C for 2 h. The reaction was cooled to RT and then stripped of dioxane. EtOAc (20 mL) was then added, and the resulting mixture was filtered through a pad of Celite. The filtrate was concentrated

to give a brown residue. This residue, dissolved in a minimal amount of DMSO and AcOH, was then loaded onto a RediSep C_{18}Aq (30 g) column primed with $H_2O+0.1\%$ AcOH. The column was then eluted with 2 CV of $H_2O+0.1\%$ AcOH and then the eluent was gradually changed to $CH_3CN+0.1\%$ AcOH over 10 CV. The fractions containing the desired product were pooled and stripped of solvent under vacuum to provide a yellow solid (**2a**, 55 mg, 28%); mp: 126–128 °C; ^{1}H NMR (400 MHz, [D_6]DMSO): $\delta=$ 2.33 (s, 3H), 2.39–2.49 (m, 5H), 3.44 (m, $J=4.40$ Hz, 4H), 3.53 (brs, 2H), 4.36–4.47 (m, 1H), 6.00 (s, 1H), 7.31–7.39 (m, 1H), 7.53 (t, $J=$ 7.83 Hz, 2H), 7.62 (d, $J=7.83$ Hz, 2H), 7.68 (s, 1H) 8.08 (d, $J=$ 1.47 Hz, 1H), 9.17–9.24 (m, 1H); IR: $\tilde{\nu}=3580$–2827 cm^{-1} (NH+OH); MS (ESI+) m/z: 380.4 $[M+H]^+$ ($C_{20}H_{25}N_7O$).

2-(4-(6-((1-Benzyl-1*H*-imidazol-4-yl)amino)-2-methylpyrimidin-4-yl)piperazin-1-yl)ethanol (2b): To *N*-(1-benzyl-1*H*-imidazol-4-yl)-6-chloro-2-methylpyrimidin-4-amine **7a** (60 mg, 0.20 mmol) in dry DMSO (1 mL), 2-(piperazin-1-yl)ethanol (0.037 mL, 0.30 mmol) and DIPEA (0.070 mL, 0.40 mmol) were added. The resulting mixture was heated at 100 °C overnight. DIPEA was then evaporated, AcOH (0.5 mL) was added, and the resulting solution was loaded onto a RediSep C_{18}Aq (30 g) column primed with $H_2O+0.1\%$ AcOH. The column was then eluted with 2 CV of $H_2O+0.1\%$ AcOH and then the eluent was gradually changed to $CH_3CN+0.1\%$ AcOH over 10 CV. The fractions containing the desired product were pooled and stripped of solvent under vacuum to give a brown solid. This solid was then loaded onto a Biotage KP-NH column (11 g) primed with CH_2Cl_2 only. The column was then run for 2 CV with CH_2Cl_2 only and then changed to CH_2Cl_2/MeOH 8:2 over 3 CV. The fractions containing the desired product were pooled and stripped of solvent under vacuum to provide, on drying under high vacuum, a yellow solid. 2-(4-(6-((1-Benzyl-1*H*-imidazol-4-yl)amino)-2-methylpyrimidin-4-yl)piperazin-1-yl)ethanol **2b** (31 mg, 40%); mp: 173–176 °C; ^{1}H NMR (400 MHz, [D_6]DMSO): $\delta=2.24$ (s, 3H), 2.38–2.48 (m, 6H), 3.36–3.45 (m, 4H), 3.49–3.56 (m, 2H), 4.41 (t, $J=5.38$ Hz, 1H), 5.15 (s, 2H), 5.96 (s, 1H), 7.14 (s, 1H), 7.26–7.40 (m, 5H), 7.55 (d, $J=1.47$ Hz, 1H), 8.97 ppm (s, 1H); IR: $\tilde{\nu}=3440$–2827 cm^{-1} (NH+OH); MS (ESI+) m/z: 394.4 $[M+H]^+$ ($C_{21}H_{27}N_7O$).

2-(4-(2-Methyl-6-((1-phenethyl-1*H*-imidazol-4-yl)amino)pyrimidin-4-yl)piperazin-1-yl)ethanol (2c): 6-Chloro-2-methyl-*N*-(1-phenethyl-1*H*-imidazol-4-yl)pyrimidin-4-amine **7b** (50 mg, 0.16 mmol), 2-(piperazin-1-yl)ethanol (0.029 mL, 0.30 mmol), and DIPEA (0.070 mL 0.40 mmol) were reacted in dry DMSO (1 mL) using the same procedure as described for the synthesis of **2b**, providing **2c** as a brown solid (16 mg, 25%); mp: 167–169 °C; ^{1}H NMR (400 MHz, [D_6]DMSO): $\delta=2.27$ (s, 3H), 2.39–2.48 (m, 6H), 3.04 (t, $J=7.34$ Hz, 2H), 3.37–3.45 (m, 4H), 3.49–3.57 (m, 2H), 4.17 (t, $J=7.09$ Hz, 2H), 4.41 (t, $J=5.38$ Hz, 1H), 5.93 (s, 1H), 7.14 (s, 1H), 7.19–7.32 (m, 6H), 8.89 ppm (s, 1H); IR: $\tilde{\nu}=3363$–2838 cm^{-1} (NH+OH); MS (ESI+) m/z: 408.4 $[M+H]^+$ ($C_{22}H_{29}N_7O$).

2-((2-Methyl-6-((1-phenethyl-1*H*-imidazol-4-yl)amino)pyrimidin-4-yl)amino)ethanol (2d): To 6-chloro-2-methyl-*N*-(1-phenethyl-1*H*-imidazol-4-yl)pyrimidin-4-amine **7b** (80 mg, 0.255 mmol) was added ethanolamine (0.020 mL, 0.33 mmol) followed by diethylene glycol monomethyl ether (2 mL). The mixture was heated at 130 °C overnight and then cooled to RT. H_2O (0.25 mL) and AcOH (0.25 mL) were added. The solution was then loaded onto a RediSep C_{18}Aq column (50 g) primed with $H_2O+0.1\%$ AcOH. The column was then eluted with 2 CV of $H_2O+0.1\%$ AcOH and then the eluent was gradually changed to $CH_3CN+0.1\%$ AcOH over 10 CV. The fractions containing the desired product were pooled and stripped of solvent under vacuum to give, on drying under high vacuum, a yellow solid **2d** (49 mg, 57%); mp: 163–165 °C; ^{1}H NMR (400 MHz, [D_6]DMSO): $\delta=2.23$ (s, 3H), 3.03 (t, $J=7.34$ Hz, 2H), 3.16–3.26 (m, 2H), 3.48 (t, $J=5.62$ Hz, 2H), 4.16 (t, $J=7.34$ Hz, 2H), 4.75 (brs, 1H), 5.73 (s, 1H), 6.47 (brs, 1H), 7.09 (s, 1H), 7.19–7.32 (m, 6H), 8.73 ppm (brs, 1H); IR: $\tilde{\nu}=3360$–2838 cm^{-1} (NH+OH); MS (ESI+) m/z: 339.3 $[M+H]^+$ ($C_{18}H_{22}N_6O$).

***N*-4-(2-Methoxyethyl)-2-methyl-*N*6-(1-phenethyl-1*H*-imidazol-4-yl)pyrimidine-4,6-diamine (2e)**: 6-Chloro-2-methyl-*N*-(1-phenethyl-1*H*-imidazol-4-yl)pyrimidin-4-amine **7b** (80 mg, 0.25 mmol) and 2-methoxyethanamine (0.029 mL, 0.33 mmol) were reacted in diethylene glycol monomethyl ether (2 mL) using the same procedure as described for the synthesis of **2d**, providing **2e** as a yellow solid (46 mg, 51%); mp: 129–131 °C; ^{1}H NMR (400 MHz, [D_6]DMSO): $\delta=$ 2.23 (s, 3H), 3.03 (s, 2H), 3.26 (s, 3H), 3.39–3.46 (m, 2H), 4.16 (t, $J=$ 7.34 Hz, 2H), 5.74 (s, 1H), 6.54 (brs, 1H), 7.08 (s, 1H), 7.19–7.32 (m, 6H), 8.71 ppm (brs, 1H), (2H under solvent peak); IR: $\tilde{\nu}=$ 3231 cm^{-1} (NH); MS (ESI+) m/z: 353.3 $[M+H]^+$ ($C_{19}H_{24}N_6O$).

2-((2-Methyl-6-((1-phenethyl-1*H*-imidazol-4-yl)amino)pyrimidin-4-yl)oxy)ethanol (2f): To 6-Chloro-2-methyl-*N*-(1-phenethyl-1*H*-imidazol-4-yl)pyrimidin-4-amine **7b** (80 mg, 0.255 mmol) was added ethylene glycol (2 mL, 0.255 mmol) followed by NaH 60% dispersion in mineral oil (30.6 mg, 1.275 mmol). Once gas evolution had stopped, the mixture was heated at 130 °C for 2 h. The mixture was then cooled to RT. H_2O (0.25 mL) and AcOH (0.25 mL) were added. The solution was then loaded onto RediSep C_{18}Aq column (50 g) primed with $H_2O+0.1\%$ AcOH. The column was then eluted with 2 CV of $H_2O+0.1\%$ AcOH and then the eluent was gradually changed to $CH_3CN+0.1\%$ AcOH over 10 CV. The fractions containing the desired product were pooled and stripped of solvent under vacuum to give, on drying under high vacuum, 2-((2-methyl-6-((1-phenethyl-1*H*-imidazol-4-yl)amino)pyrimidin-4-yl)oxy)ethanol **2f** as a white solid (65 mg, 75%); mp: 154–157 °C; ^{1}H NMR (400 MHz, [D_6]DMSO): $\delta=2.36$ (s, 3H), 3.04 (t, $J=7.34$ Hz, 2H), 3.66 (q, $J=5.38$ Hz, 2H), 4.16–4.24 (m, 4H), 4.80 (t, $J=5.62$ Hz, 1H), 6.04 (brs, 1H), 7.12–7.35 (m, 7H), 9.22–9.35 ppm (m, 1H); IR: $\tilde{\nu}=3370$–2860 cm^{-1} (NH+OH); MS (ESI+) m/z: 340.6 $[M+H]^+$ ($C_{18}H_{21}N_5O_2$).

6-(2-Ethoxyethoxy)-2-methyl-*N*-(1-phenethyl-1*H*-imidazol-4-yl)-pyrimidin-4-amine (2g): 6-Chloro-2-methyl-*N*-(1-phenethyl-1*H*-imidazol-4-yl)pyrimidin-4-amine (80 mg, 0.255 mmol) and NaH 60% dispersion in mineral oil (30.6 mg, 1.27 mmol) were reacted in ethylene glycol monoethyl ether (2 mL, 0.255 mmol) using the same procedure as described for the synthesis of **2f**, providing **2g** as a brown solid (60 mg, 60%); mp: 118–121 °C; ^{1}H NMR (400 MHz, [D_6]DMSO): $\delta=1.12$ (t, $J=6.85$ Hz, 3H), 2.36 (s, 3H), 3.04 (t, $J=$ 7.09 Hz, 2H), 3.48 (d, $J=6.85$ Hz, 2H), 3.61–3.67 (m, 2H), 4.19 (t, $J=$ 7.34 Hz, 2H), 4.28–433 (m, 2H), 6.02 (brs, 1H), 7.12–7.33 (m, 7H), 9.22–9.37 ppm (m, 1H); IR: $\tilde{\nu}=3283$ cm^{-1} (NH); MS (ESI+) m/z: 368.3 $[M+H]^+$ ($C_{20}H_{25}N_5O_2$).

2-Chloro-3-phenylpropanal (9): L-(−)-proline (8.58 mg, 0.075 mmol) was added to a stirred solution of 3-phenylpropanal (0.099 mL, 0.745 mmol) in dry CH_2Cl_2 (2 mL). The solution was cooled to 0 °C in an ice bath and then *N*-chlorosuccinimide (129 mg, 0.969 mmol) was added. The ice bath was removed and the mixture allowed to warm to RT overnight. CH_2Cl_2 was then evaporated to give 2-chloro-3-phenylpropanal **9**, which was used directly in the next step without further purification. ^{1}H NMR (400 MHz, $CDCl_3$): $\delta=3.10$ (dd, $J=14.43$, 8.07 Hz, 1H), 3.40 (dd, $J=$ 14.67, 5.87 Hz, 1H), 4.41 (ddd, $J=8.07$, 5.87, 2.20 Hz, 1H), 7.22–7.39 (m, 5H), 9.56 ppm (d, $J=1.96$ Hz, 1H).

5-Benzylthiazol-2-amine (10): 2-Chloro-3-phenylpropanal **9** (50 mg, 0.296 mol) was dissolved in EtOH (2 mL). Thiourea (113 mg, 1.491 mol) was added, and the mixture was heated at reflux for

5 h. The solvent was evaporated to dryness, and the residue was dissolved in CH_2Cl_2 (4 mL) and then washed with NaOH (10% aq, 3 mL) and H_2O (1.5 mL). The organic layer was extracted with HCl (5% aq, 3×6 mL). The combined aqueous layers were brought to pH 10 with a 10% aqueous solution of NaOH (9 mL) and then extracted with CH_2Cl_2 (3×15 mL). The organic solution was dried with Na_2SO_4 and evaporated to give an orange oil. The oil was loaded onto a Cartridge Biotage KP-NH column (55 g) primed with CyHex/EtOAc 8:2. The column was then run for 3 CV with CyHex/EtOAc 8:2 and then changed to CyHex/EtOAc 1:1 over 5 CV. The fractions containing the desired product were pooled and stripped of solvent under vacuum to obtain 5-benzylthiazol-2-amine **10** as a yellow oil (23 mg, 16%). MS (ESI+) *m/z*: 190.9 $[M+H]^+$ ($C_{10}H_{10}N_2S$).

2-(4-(6-Chloro-2-methylpyrimidin-4-yl)piperazin-1-yl)ethanol (11): 4,6-Dichloro-2-methylpyrimidine (5 g, 30.7 mmol) and 2-(piperazin-1-yl)ethanol (7.99 g, 61.30 mmol) were mixed in CH_2Cl_2 (40 mL) and stirred at 30 °C overnight. After vacuum filtration, the filtrate was vacuum dried. *n*-Hexane (20 mL) was then added. The suspension so obtained was filtered, and the solid was dried at 45 °C under vacuum to give 2-(4-(6-chloro-2-methylpyrimidin-4-yl)-piperazin-1-yl)ethanol **11** as a white solid (7.91 g, 100%); mp: 70–72 °C; ^{1}H NMR (400 MHz, $CDCl_3$): $\delta = 2.50$ (s, 3H), 2.60–2.68 (m, 6H), 3.72 (t, $J = 5.38$ Hz, 6H), 6.35 ppm (s, 1H); IR: $\tilde{\nu} = 3589$–2827 cm^{-1} (OH); MS (ESI+) *m/z*: 257.1 $[M+H]^+$ ($C_{11}H_{17}ClN_4O$).

2-(4-(6-((5-Benzylthiazol-2-yl)amino)-2-methylpyrimidin-4-yl)piperazin-1-yl)ethanol (3a): To 4,5-Bis(diphenylphosphino)-9,9-dimethylxanthene (6.99 mg, 0.012 mmol), tris(dibenzylideneacetone)dipalladium(0) (3.32 mg, 3.63 μmol), 5-benzylthiazol-2-amine (23 mg, 0.121 mmol) and 2-(4-(6-chloro-2-methylpyrimidin-4-yl)piperazin-1-yl)ethanol (34.1 mg, 0.133 mmol), dry dioxane (3 mL) was added. The reaction was heated at 100 °C for 4 h. The reaction was cooled to RT, volatiles were evaporated off, and the crude was treated with CH_2Cl_2 (15 mL) and H_2O (20 mL). The organic phase was dried with Na_2SO_4, filtered and evaporated under reduced pressure. The crude so obtained was dissolved in DMSO (1 mL) and acidified with AcOH (0.4 mL). The resulting solution was loaded onto a RediSep C_{18}Aq column (30 g) primed with H_2O + 0.1% AcOH. The column was then eluted with 2 CV of H_2O + 0.1% AcOH, and then the eluent was gradually changed to CH_3CN + 0.1% AcOH over 10 CV. The fractions containing the desired product were pooled and stripped of solvent under vacuum to obtain, on drying under high vacuum, a brown solid **3a** (20 mg, 40%); mp: 208–210 °C; ^{1}H NMR (400 MHz, [D$_6$]DMSO): $\delta = 2.31$ (s, 3H), 2.39–2.48 (m, 6H), 3.47 (br s, 4H), 3.53 (q, $J = 5.71$ Hz, 2H), 4.05 (s, 2H), 4.41 (br s, 1H), 6.03 (s, 1H), 7.11 (s, 1H), 7.23–7.35 (m, 5H), 10.84–10.92 ppm (m, 1H); IR: $\tilde{\nu} = 3603$–2827 cm^{-1} (NH + OH); MS (ESI+) *m/z*: 411 $[M+H]^+$ ($C_{21}H_{26}N_6OS$).

***N*-(6-Chloro-2-methylpyrimidin-4-yl)-5-phenylthiazol-2-amine (14)**: To 4,5-Bis(diphenylphosphino)-9,9-dimethylxanthene (98 mg, 0.170 mmol) and tris(dibenzylideneacetone)dipalladium(0) (46.8 mg, 0.051 mmol), 5-phenylthiazol-2-amine (300 mg, 1.702 mmol) and 4,6-dichloro-2-methylpyrimidine (277 mg, 1.702 mmol), dry dioxane (8 mL) was added. The mixture was heated at 95 °C overnight. The reaction was cooled to RT, volatiles were evaporated off, and the crude was treated with CH_2Cl_2 (10 mL) and filtered through a pad of Celite. The filtrate was evaporated under reduced pressure and then loaded onto a Biotage HP-SiO_2 (100 g) column primed with CyHex/EtOAc 8:2. The column was then run for 2 CV with CyHex/EtOAc 8:2 and then changed to EtOAc over 10 CV. The fractions containing the desired product were pooled and stripped of solvent to give, on drying under vacuum, *N*-(6-chloro-2-methylpyrimidin-4-yl)-5-phenylthiazol-2-amine **14** as a yellow solid (390 mg, 76%). ^{1}H NMR (400 MHz, [D$_6$]DMSO): $\delta = 2.39$ (s, 3H), 6.90 (s, 1H), 7.35–7.41 (m, 1H), 7.45 (t, $J = 7.58$ Hz, 2H), 7.88 (d, $J = 1.47$ Hz, 2H), 7.64 (s, 1H), 9.47 ppm (br s, 1H); MS (ESI+) *m/z*: 303.1 $[M+H]^+$ ($C_{14}H_{11}ClN_4S$).

2-(4-(2-Methyl-6-((5-phenylthiazol-2-yl)amino)pyrimidin-4-yl)piperazin-1-yl)ethanol (3b): To a solution of *N*-(6-chloro-2-methylpyrimidin-4-yl)-5-phenylthiazol-2-amine **14** (60 mg, 0.198 mmol) in dry DMSO (1.5 mL), 2-(piperazin-1-yl)ethanol (38.7 mg, 0.297 mmol) followed by DIPEA (0.104 mL, 0.594 mmol) were added. The resulting mixture was heated at 80 °C for 18 h. The reaction was cooled to RT, and then the DIPEA was removed under vacuum. To the remaining solution AcOH (0.5 mL) was added and then it was loaded onto RediSep C_{18}Aq column (30 g) primed with H_2O + 0.1% AcOH. The column was then eluted with 2 CV of H_2O + 0.1% AcOH and then the eluent was gradually changed to CH_3CN + 0.1% AcOH over 10 CV. The fractions containing the desired product were pooled and stripped of solvent under vacuum to obtain, on drying under high vacuum, a white solid. 2-(4-(2-Methyl-6-((5-phenylthiazol-2-yl)amino)pyrimidin-4-yl)piperazin-1-yl)ethanol (**3b**; 60 mg, 76%); mp: 258–260 °C; ^{1}H NMR (400 MHz, [D$_6$]DMSO): $\delta = 2.40$–2.49 (m, 8H), 3.46–3.58 (m, 6H), 4.43 (t, $J = 5.38$ Hz, 1H), 6.06 (s, 1H), 7.27 (s, 1H) 7.40 (t, $J = 7.58$ Hz, 2H), 7.59 (dd, $J = 8.07$, 1.22 Hz, 2H), 7.76 (s, 1H), 11.07–11.21 ppm (m, 1H), (1H under the solvent peak); IR: $\tilde{\nu} = 3605$–2800 cm^{-1} (NH + OH); MS (ESI+) *m/z*: 397.3 $[M+H]^+$ ($C_{20}H_{24}N_6OS$).

2-((2-Methyl-6-((5-phenylthiazol-2-yl)amino)pyrimidin-4-yl)amino)ethanol (3c): To *N*-(6-chloro-2-methylpyrimidin-4-yl)-5-phenylthiazol-2-amine **14** (80 mg, 0.264 mmol), ethanolamine (96 μL, 1.585 mmol) was added. Then diethylene glycol monomethyl ether (2 mL) was added. The reaction was heated at 100 °C overnight. The mixture was cooled to RT and then H_2O (0.30 mL) and AcOH (0.30 mL) were added. The solution was then loaded onto a RediSep C_{18}Aq column (30 g) primed with H_2O + 0.1% AcOH. The column was then eluted with 2 CV of H_2O + 0.1% AcOH and then the eluent was gradually changed to CH_3CN + 0.1% AcOH over 10 CV. The fractions containing the desired product were pooled and stripped of solvent under vacuum to provide, on drying under high vacuum, 2-((2-methyl-6-((5-phenylthiazol-2-yl)amino)pyrimidin-4-yl)amino)ethanol **3c** as a white solid (13 mg, 15.03%); mp: 251–253 °C; ^{1}H NMR (400 MHz, [D$_6$]DMSO): $\delta = 2.38$ (s, 3H), 3.51 (q, $J = 5.87$ Hz, 2H), 4.72 (t, $J = 5.38$ Hz, 1H), 5.90 (br s, 1H), 6.97–7.09 (m, 1H), 7.26 (s, 1H), 7.40 (t, $J = 7.83$ Hz, 2H), 7.58 (d, $J = 7.83$ Hz, 2H), 7.74 (s, 1H), 11.01–11.11 ppm (m, 1H), (2H under the solvent peak); IR: $\tilde{\nu} = 3605$–2700 cm^{-1} (NH + OH); MS (ESI+) *m/z*: 327.9 $[M+H]^+$ ($C_{16}H_{17}N_5OS$).

***N*-4-(2-Methoxyethyl)-2-methyl-*N*6-(5-phenylthiazol-2-yl)pyrimidine-4,6-diamine (3d)**: *N*-(6-chloro-2-methylpyrimidin-4-yl)-5-phenylthiazol-2-amine **14** (80 mg, 0.264 mmol) and 2-methoxyethanamine (138 μL, 1.585 mmol) were reacted followed the same procedure of **3c** to provide *N*-4-(2-methoxyethyl)-2-methyl-*N*6-(5-phenylthiazol-2-yl)pyrimidine-4,6-diamine **3d** (22 mg, 24.39%) as a yellow solid; mp: 225–227 °C; ^{1}H NMR (400 MHz, [D$_6$]DMSO): $\delta = 2.39$ (s, 3H), 3.28 (s, 3H), 3.36–3.4 (m, 4H), 5.91 (s, 1H), 7.12 (br s, 1H), 7.23–7.29 (m, 1H), 7.40 (t, $J = 7.83$ Hz, 2H), 7.58 (d, $J = 7.34$ Hz, 2H), 7.74 (s, 1H), 11.05 ppm (s, 1H); IR: $\tilde{\nu} = 3234$ cm^{-1} (NH); MS (ESI+) *m/z*: 342.2 $[M+H]^+$ ($C_{17}H_{19}N_5OS$).

2-((2-Methyl-6-((5-phenylthiazol-2-yl)amino)pyrimidin-4-yl)oxy)-ethanol (3e): To *N*-(6-chloro-2-methylpyrimidin-4-yl)-5-phenylthiazol-2-amine **14** (94 mg, 0.310 mmol) ethylene glycol (2 mL, 0.310 mmol) was added. Then a NaH 60% dispersion in mineral oil

(37.3 mg, 1.552 mmol) was added. Once gas evolution had stopped, the mixture was heated at 130 °C overnight. The mixture was cooled to RT and then H_2O (0.30 mL) and AcOH (0.30 mL) were added. This mixture was then loaded onto RediSep C_{18}Aq column (50 g) primed with H_2O + 0.1% AcOH. The column was then eluted with 2 CV of H_2O + 0.1% AcOH and then the eluent was gradually changed to CH_3CN + 0.1% AcOH over 10 CV. The fractions containing the desired product were pooled and stripped of solvent under vacuum to obtain, on drying under high vacuum, 2-((2-methyl-6-((5-phenylthiazol-2-yl)amino)pyrimidin-4-yl)oxy)ethanol **3e** (15 mg, 14.71%) as a white solid; mp: 239–241 °C; ^{1}H NMR (400 MHz, [D_6]DMSO): δ = 2.53 (s, 3H), 3.70 (t, J = 5.14 Hz, 2H), 4.30 (t, J = 5.14 Hz, 2H), 4.85 (br s, 1H), 6.25 (s, 1H), 7.26–7.32 (m, 1H), 7.42 (t, J = 7.58 Hz, 2H), 7.61 (d, J = 7.34 Hz, 2H), 7.81 (s, 1H), 11.48 ppm (s, 1H); IR: $\tilde{\nu}$ = 3600–2780 cm^{-1} (NH + OH); MS (ESI+) m/z: 329.2 $[M+H]^+$ ($C_{16}H_{16}N_4O_2S$).

***N*-(6-(2-Ethoxyethoxy)-2-methylpyrimidin-4-yl)-5-phenylthiazol-2-amine (3f)**: *N*-(6-chloro-2-methylpyrimidin-4-yl)-5-phenylthiazol-2-amine **14** (94 mg, 0.310 mmol), ethylene glycol monoethyl ether (2 mL, 0.310 mmol) and NaH 60% dispersion in mineral oil (37.3 mg, 1.552 mmol) were reacted following the same procedure of **3e** to provide *N*-(6-(2-ethoxyethoxy)-2-methylpyrimidin-4-yl)-5-phenylthiazol-2-amine **3f** (13 mg, 11.75%) as a white solid; mp: 202-203.5 °C; ^{1}H NMR (400 MHz, [D_6]DMSO): δ = 1.13 (t, J = 7.09 Hz, 3H), 2.53 (s, 3H), 3.46–3.53 (m, 2H), 3.69 (d, J = 4.40 Hz, 2H), 4.38–4.42 (m, 2H), 6.24 (s, 1H), 7.29 (s, 1H), 7.39–7.44 (m, 2H), 7.61 (d, J = 7.34 Hz, 2H), 7.81 (s, 1H), 11.49 ppm (s, 1H); IR: $\tilde{\nu}$ = 3274 cm^{-1} (NH); MS (ESI+) m/z: 357.3 $[M+H]^+$ ($C_{18}H_{20}N_4O_2S$).

Enzyme assays

Assays to determine the kinase inhibitory activity of test compounds were performed using an automatic liquid-handling device (Microlab STAR Hamilton) and Z′-LYTE Kinase Assay Platform, a fluorescence resonance energy transfer (FRET)-based assay platform compatible with high-throughput screening (HTS) applications. The assay has a fluorescence-based, coupled-enzyme format and uses the differential sensitivities of phosphorylated and non-phosphorylated peptides toward proteolytic cleavage. The assay procedure was carried out according to the supplier's indications. Test compounds were evaluated in a primary screen against active human recombinant Src (62.3 kDa), followed by an off-target profiling assay toward a selected panel of Src family kinases (Fyn, Lyn A and Yes 1, all human recombinant full-length proteins). The final enzyme concentrations were 4, 9, 0.9, and 3 nM for Src, Fyn, Lyn 6A and Yes 1, respectively. The desired enzyme was incubated in a 384-well low-volume microplate with a synthetic peptide substrate, ATP, and various final inhibitor concentrations, ranging from 10^{-10} M to 10^{-5} M (8–10 data points in duplicate for each curve). Samples representing 0% inhibition (or total enzymatic activity) were run in the presence of compound diluent (1% DMSO, final) in reaction buffer (50 mM HEPES, 10 mM $MgCl_2$, 1 mM EGTA, 0.01% Brij-35, pH 7.5). Near-K_M ATP concentrations for each kinase and an optimal enzyme concentration that phosphorylates 20–40% of the Z′-LYTE Tyr 2 peptide in a 1 h incubation were selected. All reagents were diluted in reaction buffer, and the kinase reaction was carried out in a total volume of 10 μL for 60 min at 25 °C. No (0%) phosphorylation (i.e., no ATP) and full (100%) phosphorylation (i.e., synthetically phosphorylated peptide supplied) assay controls, included in each plate, allowed the calculation of the percent phosphorylation achieved in a given specific reaction well. The 0% inhibition and 0% phosphorylation (i.e., 100% inhibition) controls define the dynamic range in the screen. At the end of kinase reaction, a secondary reaction (development reaction) was started by adding 5 μL of development reagent, containing a site-specific protease that recognizes and cleaves non-phosphorylated peptides, and was interrupted after 60 min with stop reagent (5 μL per sample). Measurement of coumarin (λ_{ex} 400 nm, λ_{em} 460 nm) and fluorescein (λ_{ex} 400 nm, λ_{em} 535 nm) signals was performed with a fluorescence plate reader (Envision, PerkinElmer). Final results are expressed as percent inhibition, and IC_{50} values were calculated by nonlinear curve fitting using GraphPad Prism software (version 6 for Windows). The inter-experimental variability of IC_{50} values is within accepted limits of ±0.5 log units.

Molecular modeling

Protein preparation: Crystal structures of c-Src and Lyn in complex with dasatinib (PDB IDs: 3G5D[40] and 2ZVA,[42] respectively), Fyn in complex with staurosporine (PDB ID: 2DQ7),[43] and c-Src in complex with AP23464 (PDB ID: 2BDJ2BDJ) and CGP77675 (PDB ID: 1YOL) were retrieved from the RCSB Protein Data Bank. After removal of bound ligands, the proteins were prepared by using the Protein Preparation Wizard[40] workflow (Schrödinger). In particular, all water molecules were deleted, hydrogen atoms were added, and partial charges were assigned. In addition, the ionization and tautomeric states of His, Asp, Glu, Arg, and Lys were adjusted to match pH 7.4. Next, optimization of the hydrogen bonding network was obtained by reorienting hydroxy and thiol groups, amide groups of Asn and Gln, and the His imidazole ring. Finally, the system was refined by running a restrained minimization (OPLS2005 force field) which was stopped when the RMSD of heavy atoms reached 0.30 Å, the default specified limit.

Ligand preparation: All compounds were drawn and minimized using Maestro 9.2[41] and MacroModel[48] (Schrödinger), respectively. Furthermore, LigPrep[49] was used to predict ionization and tautomeric states for the ligands using pH 7 ± 0.5.

Homology modeling: The FASTA sequences of Fyn and Yes were used in turn as queries, the coordinates of c-Src crystal structure bound by dasatinib and the missing residues were built by using the program Prime.[40] For each structure, the serial loop sampling approach was applied by choosing "Extended" as level of accuracy (recommended for loop length between 6 and 11 residues), and the lowest-energy conformation was saved for the next analysis. The maximum number of structures to return was set to 10. An energy cutoff of 10 kcal mol^{-1} was applied. Loop conformations were clustered, and representatives of each cluster were selected. The best-scoring loop structure was finally selected.

Docking studies: Docking simulations were performed using the Glide program[37,38] within the ATP binding sites of Src, Lyn, Fyn, and Yes. The prepared protein systems were used to generate the receptor grids, and no scaling was done for van der Waals (vdW) radii of nonpolar receptor atoms. A grid box of default size was centered on the X-ray ligand. No constraints were included during grid generation while rotation of the hydroxy groups was allowed. After grid preparation, compounds were flexibly docked and scored using the Glide standard-precision (SP) mode, treating the proteins as rigid. Docking experiments were performed using 0.80 factor to scale vdW radii of the nonpolar ligand atoms with a partial atomic charge of < 0.15.

Molecular dynamics: MD simulations were performed by starting from the best docking poses of selected compounds within the ATP binding site of Src according to a previously reported procedure.[50] Standard AMBER12 ff99SB force field for bioorganic sys-

tems was used to describe the protein parameters. Each complex was placed in a cubic box of TIP3P water molecules, and an appropriate number of counterions (nine Na^+ ions) were added. The distance between the box walls and the protein was set to 13 Å. Before MD simulations, two steps of energy minimization were performed to remove bad contacts. In the first stage, the protein was kept fixed with a constraint of 500 kcal mol^{-1}, and only the water molecules were minimized. In the second stage, the entire system was minimized applying a constraint of 10 kcal mol^{-1} on the α-carbon. The two minimization stages consisted of 5000 steps in which the first 1000 were steepest descent and the last were conjugate gradient. MD trajectories were run using the minimized structures as a starting point. Constant-volume simulations were performed for 500 ps, during which the temperature was raised from 0 to 300 K using the Langevin dynamics method. Then 1500 ps of constant-pressure MD simulations were performed at 300 K in three steps of 500 ps each. During these steps a decreasing harmonic force constraint of 10, 5, and 1 kcal mol^{-1} Å^{-1} was applied respectively. Finally, 50 ns MD simulations for ligands without restraints were run at constant temperature (300 K) and constant pressure (1 atm). During the simulations, the particle mesh Ewald method was used to calculate long-range electrostatic interactions. A 10 Å cutoff value was used for the non-bonded interactions, and a time step of 2 fs was used for the simulations.

Analysis of MD trajectories: The module Ptraj implemented in AMBER12 was used to analyze trajectories. In particular, root-mean-square deviation (RMSD) and root-mean-square fluctuation (RMSF) were calculated for the α-carbons of each residue on the production stage. During the simulation, the hydrogen bonds between the ligands and receptor were detected when the acceptor–donor atom distance was <3.5 Å and the occupancy was $>10\%$ in the investigated time period.

MM/GBSA analysis: The MM/GBSA approach was used to evaluate the binding free energy between the preferred poses of ligands and the protein. This method estimates the ΔG_{bind} as the difference in free energy between the complex (PL), the ligand (L) and the receptor (P) Eq. (1).

$$\Delta G_{bind} = G(PL) - G(P) - G(L) \quad (1)$$

Each binding free energy term in Eq. (1) was estimated from the following Eq. (2):

$$\Delta G = \Delta G_{MM} + \Delta G_{solv} - T\Delta S \quad (2)$$

in which ΔG_{MM} (molecular mechanics) is the gas-phase energy, calculated by Eq. (3) as the sum of electrostatic and van der Waals interaction energies; ΔG_{solv} is the solvation free energy and was calculated with Eq. (4), whereas the final term is the absolute temperature multiplied by the estimated entropy. The entropy term was considered negligible and was therefore not calculated in this work, thus sparing the high computational expenses.

$$\Delta G_{MM} = \Delta G_{ele} + \Delta G_{vdW} \quad (3)$$

The solvation free energy was composed of polar and nonpolar contributions:

$$\Delta G_{solv} = \Delta G_{ele,solv} + \Delta G_{nonpol,solv} \quad (4)$$

for which the polar part $\Delta G_{ele,solv}$ was calculated by solving the Poisson–Boltzmann (PB)[51] equation in the case of the MM/PBSA method or the generalized Born (GB)[52] model with MM/GBSA. The nonpolar solvation was estimated with Eq. (5) by calculating the solvent accessible surface area (SASA) with the AMBER11 molsurf module:

$$G_{nonpol} = \gamma \times SASA + b \quad (5)$$

In detail, SASA was determined by recursively approximating a sphere around each atom, starting from icosahedra (ICOSA method). The radius of the probe sphere used to calculate the SASA was set at 0.0. The surface tension proportionality constant γ, and the free energy of nonpolar solvation for a point solute b were set at 0.0072 kcal mol^{-1} Å^{-2} and 0.00 kcal mol^{-1}, respectively. Binding free energies were calculated on systems in which water molecules used during the simulation were stripped off, with the exception of selected water molecules involved in interactions with the ligands. Only the complex PL was simulated, and the free energies of P and L were obtained from the same simulation by simply deleting the coordinates of the other species, as well as generally made. The final 6 ns of our simulations were regarded as stable and were used to extract 150 snapshots from each trajectory. The ligand–protein binding free energy (ΔG_{bind}) for each snapshot was then estimated using Eq. (1).

Cell proliferation analysis: In vitro experiments were carried out using the human neuroblastoma cell line SH-SY5Y and leukemia cell line K562. Cells were purchased from the American Type Culture Collection (ATCC, Manassas, VA, USA) and were cultured in DMEM supplemented with 10% fetal bovine serum. To determine the antiproliferative effect of drugs, tumor cells were seeded at a density of 2×10^5 cells per mL and treated with compounds at increasing concentrations from 0.01 to 10 μM. The cultures were maintained at 37 °C in 5% *v/v* CO_2 for 72 h. Cell number and vitality were evaluated using an automated cell counter (NucleoCounter, Chemometec, Denmark). Results from the NucleoCounter represented either total or nonviable cell concentration, depending on the sample preparation indicated by the manufacturer.

Cell-cycle analysis: Cells in exponential growth were treated with selected inhibitors at a density of 1×10^6 cells per mL for 48 h. At the endpoint, at least 5×10^6 cells were harvested, washed with phosphate-buffered saline (PBS) and fixed overnight with 70% EtOH. The EtOH was then removed by centrifugation (600 *g*, 5 min, 4 °C), and the cells were resuspended in PBS, stained with 50 μg mL^{-1} propidium iodide (PI) at 4 °C for 30 min in the dark. Stained cells were analyzed by Tali image-based cytometer (Life Technologies, Carlsbad, CA, USA) counting 20 fields for each sample, and exported .fcs raw data files were elaborated by Flowing software (version 2.5.0, Perttu Terho, University of Turku, Finland).

Acknowledgements

This work was supported in part by the National Interest Research Project PRIN 2010 5YY2HL. Rottapharm Biotech and Lead Discovery Siena S.r.l. are also acknowledged for financial support.

Keywords: aminoimidazoles · aminothiazoles · antitumor agents · inhibitors · Src kinase

[1] D. S. Krause, R. A. Van Etten, *N. Engl. J. Med.* **2005**, *353*, 172 – 187.
[2] B. D. Manning, A. M. VanHook, *Sci. Signaling* **2009**, *2*, pe15.
[3] M. Herbrink, B. Nuijen, J. H. Schellens, J. H. Beijnen, *Cancer Treat. Rev.* **2015**, *41*, 412 – 422.

[4] W. Xu, A. Doshi, M. Lei, M. J. Eck, S. C. Harrison, *Mol. Cell* **1999**, *3*, 629 – 638.
[5] S. M. Thomas, J. S. Brugge, *Annu. Rev. Cell Dev. Biol.* **1997**, *13*, 513 – 609.
[6] M. C. Frame, *Biochim. Biophys. Acta* **2002**, *1602*, 114 – 130.
[7] F. Musumeci, S. Schenone, C. Brullo, M. Botta, *Future Med. Chem.* **2012**, *4*, 799 – 822.
[8] C. Tintori, A. L. Fallacara, M. Radi, C. Zamperini, E. Dreassi, E. Crespan, G. Maga, S. Schenone, F. Musumeci, C. Brullo, A. Richters, F. Gasparrini, A. Angelucci, C. Festuccia, S. Delle Monache, D. Rauh, M. Botta, *J. Med. Chem.* **2015**, *58*, 347 – 361.
[9] S. Li, *Leuk. Lymphoma* **2008**, *49*, 19 – 26.
[10] J. H. Hanke, J. P. Gardner, R. L. Dow, P. S. Changelian, W. H. Brissette, E. J. Weringer, B. A. Pollok, P. A. Connelly, *J. Biol. Chem.* **1996**, *271*, 695 – 701.
[11] J. Bain, L. Plater, M. Elliott, N. Shpiro, C. J. Hastie, H. McLauchlan, I. Klevernic, J. S. Arthur, D. R. Alessi, P. Cohen, *Biochem. J.* **2007**, *408*, 297 – 315.
[12] K. R. Brandvold, M. E. Steffey, C. C. Fox, M. B. Soellner, *ACS Chem. Biol.* **2012**, *7*, 1393 – 1398.
[13] L. F. Hennequin, J. Allen, J. Breed, J. Curwen, M. Fennell, T. P. Green, C. L. van der Brempt, R. Morgentin, R. A. Norman, A. Olivier, L. Otterbein, P. A. Plé, N, Warin, G. Costello, *J. Med. Chem.* **2006**, *49*, 6465 – 6488.
[14] M. W. Martin, J. Newcomb, J. J. Nunes, D. C. McGowan, D. M. Armistead, C. Boucher, J. L. Buchanan, W. Buckner, L. Chai, D. Elbaum, L. F. Epstein, T. Faust, S. Flynn, P. Gallant, A. Gore, Y. Gu, F. Hsieh, X. Huang, J. H. Lee, D. Metz, S. Middleton, D. Mohn, K. Morgenstern, M. J. Morrison, P. M. Novak, A. Oliveira-dos-Santos, D. Powers, P. Rose, S. Schneider, S. Sell, Y. Tudor, S. M. Turci, A. A. Welcher, R. D. White, D. Zack, H. Zhao, L. Zhu, X. Zhu, C. Ghiron, P. Amouzegh, M. Ermann, J. Jenkins, D. Johnston, S. Napier, E. Power, *J. Med. Chem.* **2006**, *49*, 4981 – 4991.
[15] R. L. Panek, G. H. Lu, S. R. Klutchko, B. L. Batley, T. K. Dahring, J. M. Hamby, H. Hallak, A. M. Doherty, J. A. Keiser, *J. Pharmacol. Exp. Ther.* **1997**, *283*, 1433 – 1444.
[16] Y. Wang, J. Li, R. N. Booher, A. Kraker, T. Lawrence, W. R. Leopold, Y. Sun, *Cancer Res.* **2001**, *61*, 8211 – 8217.
[17] O. Hashimoto, M. Shinkawa, T. Torimura, T. Nakamura, K. Selvendiran, M. Sakamoto, H. Koga, T. Ueno, M. Sata, *BMC Cancer* **2006**, *6*, 292 – 303.
[18] D. H. Boschelli, F. Ye, Y. D. Wang, M. Dutia, S. L. Johnson, B. Wu, K. Miller, D. W. Powell, D. Yaczko, M. Young, M. Tischler, K. Arndt, C. Discafani, C. Etienne, J. Gibbons, J. Grod, J. Lucas, J. M. Weber, F. Boschelli, *J. Med. Chem.* **2001**, *44*, 3965 – 3977.
[19] M. Lindauer, A. Hochhau, *Recent Res. Dev. Cancer* **2014**, *201*, 27 – 65.
[20] O. Hantschel, U. Rix, U. Schmidt, T. Bürckstümmer, M. Kneidinger, G. Schütze, J. Colinge, K. L. Bennett, W. Ellmeier, P. Valent, G. Superti-Furga, *Proc. Natl. Acad. Sci. USA* **2007**, *104*, 13283 – 13288.
[21] M. I. Davis, J. P. Hunt, S. Herrgard, P. Cierci, L. M. Wodicka, G. Pallares, M. Hocker, D. K. Treiber, P. P. Zarrinkar, *Nat. Biotechnol.* **2011**, *29*, 1046 – 1051.
[22] J. Zhang, P. L. Yang, N. S. Gray, *Nat. Rev. Cancer* **2009**, *9*, 28 – 39.
[23] A. M. Aronov, M. A. Murcko, *J. Med. Chem.* **2004**, *47*, 5616 – 5619.
[24] Q. Su, S. Ioannidis, C. Chuaqui, L. Almeida, M. Alimzhanov, G. Bebernitz, K. Bell, M. Block, T. Howard, S. Huang, D. Huszar, J. A. Read, C. R. Costa, J. Shi, M. Su, M. Ye, M. Zinda, *J. Med. Chem.* **2014**, *57*, 144 – 158.
[25] D. Bebbington, J.-D. Charrier, R. Davies, S. Everitt, D. Kay, R. Knegtel, S. Patel (Vertex Pharmaceuticals, Inc.) Int. PCT Pub. No. WO 2002050065 A3, **2002**.
[26] J. Das, P. Chen, D. Norris, R. Padmanabha, J. Lin, R. V. Moquin, Z. Shen, L. S. Cook, A. M. Doweyko, S. Pitt, S. Pang, D. R. Shen, Q. Fang, H. F. De Fex, K. W. McIntyre, D. J. Shuster, K. M. Gillooly, K. Behnia, G. L. Schieven, J. Wityak, J. C. Barrish, *J. Med. Chem.* **2006**, *49*, 6819 – 6832.
[27] L. J. Lombardo, F. Y. Lee, P. Chen, D. Norris, J. C. Barrish, K. Behnia, S. Castaneda, L. A. M. Cornelius, J. Das, A. M. Doweyko, C. Fairchild, J. T. Hunt, I. Inigo, K. Johnston, A. Kamath, D. Kan, H. Klei, P. Marathe, S. Pang, R. Peterson, S. Pitt, G. L. Schieven, R. J. Schmidt, J. Tokarski, M. L. Wen, J. Wityak, R. M. Borzilleri, *J. Med. Chem.* **2004**, *47*, 6658 – 6661.
[28] T. K. Sawyer, R. S. Bohacek, C. A. Metcalf III, W. C. Shakespeare, Y. Wang, R. Sundaramoorthi, T. Keenan, S. Narula, M. Weigele, D. C. Dalgarno, *BioTechniques* **2003**, *34*, S2 – S15.
[29] N. Bell, C. Carreras, H.-T. Chang, D. Charmot, T. Chen, X. Du, J. W. Jacobs, E. Labonte, M. R. Leadbetter, J. G. Lewis, M. Navre, J. Oslob, N. Reich (Ardelyx, Inc.), WO 2012006475 A1, **2012**.
[30] R. Yan, H. Yang, W. Hou, Y. Xu (Nan Jing Cavendish Bio-Engineering Technology Co., Ltd.), Int. PCT Pub. No. WO 2011095126 A1, **2011**.
[31] M. T. Miller, R. S. S. Hadida, A. K. Singh, T. Cleveland, L. R. Makings, M. Hamilton, P. D. J. Grootenhuis (Vertex Pharmaceuticals, Inc.), Int. PCT Pub. No. WO 2005026137 A2, **2005**.
[32] Y. Jia, C. M. Quinn, S. Kwak, R. V. Talanian, *Curr. Drug Discovery Technol.* **2008**, *5*, 59 – 69.
[33] W. Xu, S. C. Harrison, M. J. Eck, *Nature* **1997**, *385*, 595 – 602.
[34] S. S. Taylor, A. P. Kornev, *Trends Biochem. Sci.* **2011**, *36*, 65 – 77.
[35] R. Roskoski, *Biochem. Biophys. Res. Commun.* **2004**, *324*, 1155 – 1164.
[36] Y. Meng, B. Roux, *J. Mol. Biol.* **2014**, *426*, 423 – 435.
[37] R. A. Friesner, J. L. Banks, R. B. Murphy, T. A. Halgren, J. J. Klicic, D. T. Mainz, M. P. Repasky, E. H. Knoll, M. Shelley, J. K. Perry, D. E. Shaw, P. Francis, P. S. Shenkin, *J. Med. Chem.* **2004**, *47*, 1739 – 1749.
[38] T. A. Halgren, R. B. Murphy, R. A. Friesner, H. S. Beard, L. L. Frye, W. T. Pollard, J. L. Banks, *J. Med. Chem.* **2004**, *47*, 1750 – 1759.
[39] M. Getlik, C. Grutter, J. R. Simard, S. Kluter, M. Rabiller, H. B. Rode, A. Robubi, D. Rauh, *J. Med. Chem.* **2009**, *52*, 3915 – 3926.
[40] Schrödinger Suite 2011 Protein Preparation Wizard: *Epik* version 2.2; *Impact* version 5.7; *Prime* version 3.0, Schrödinger LLC, New York, NY (USA), **2011**.
[41] *Maestro* version 9.2, Schrödinger LLC, New York, NY (USA), **2011**.
[42] N. K. Williams, I. S. Lucet, S. P. Klinken, E. Ingley, J. Rossjohn, *J. Biol. Chem.* **2009**, *284*, 284 – 291.
[43] T. Kinoshita, M. Matsubara, H. Ishiguro, K. Okita, T. Tada, *Biochem. Biophys. Res. Commun.* **2006**, *346*, 840 – 844.
[44] T. Tuccinardi, M. Botta, A. Giordano, A. Martinelli, *J. Chem. Inf. Model.* **2010**, *50*, 1432 – 1441.
[45] C. N. Cavasotto, S. S. Phatak, *Drug Discovery Today* **2009**, *14*, 676 – 683.
[46] M. Navarra, M. Celano, J. Maiulo, S. Schenone, M. Botta, A. Angelucci, P. Bramanti, D. Russo, *BMC Cancer* **2010**, *10*, 602.
[47] F. Carraro, A. Naldini, A. Pucci, G. A. Locatelli, G. Maga, S. Schenone, O. Bruno, A. Ranise, F. Bondavalli, C. Brullo, P. Fossa, G. Menozzi, L. Mosti, M. Modugno, C. Tintori, F. Manetti, M. Botta, *J. Med. Chem.* **2006**, *49*, 1549 – 1561.
[48] *MacroModel* version 9.9, Schrödinger LLC, New York, NY (USA), **2011**.
[49] *LigPrep* version 2.5, Schrödinger LLC, New York, NY (USA), **2011**.
[50] C. Tintori, N. Veljkovic, V. Veljkovic, M. Botta, *Proteins Struct. Funct. Bioinf.* **2010**, *78*, 3396 – 3408.
[51] W. Rocchia, E. Alexov, B. Honig, *J. Phys. Chem. B* **2001**, *105*, 6507 – 6514.
[52] A. Onufriev, D. Bashford, D. A. Case, *Proteins Struct. Funct. Bioinf.* **2004**, *55*, 383 – 394.

Received: September 17, 2015
Published online on October 30, 2015